Am J Cancer Res 2023;13(7):2790-2813
www.ajcr.us /ISSN:2156-6976/ajcr0150876

Original Article

Autotaxin production in the human breast cancer tumor microenvironment mitigates tumor progression in early breast cancers

Matthew GK Benesch[1*], Rongrong Wu[1,2*], Xiaoyun Tang[3], David N Brindley[3], Takashi Ishikawa[2], Kazuaki Takabe[1,2,4,5,6,7]

[1]Department of Surgical Oncology, Roswell Park Comprehensive Cancer Center, Buffalo, New York 14263, USA; [2]Department of Breast Surgery and Oncology, Tokyo Medical University, Tokyo 160-8402, Japan; [3]Cancer Research Institute of Northern Alberta, Department of Biochemistry, University of Alberta, Edmonton, Alberta T6G 2H7, Canada; [4]Department of Gastroenterological Surgery, Yokohama City University Graduate School of Medicine, Yokohama 236-0004, Japan; [5]Division of Digestive and General Surgery, Niigata University Graduate School of Medical and Dental Sciences, Niigata 951-8520, Japan; [6]Department of Breast Surgery, Fukushima Medical University School of Medicine, Fukushima 960-1295, Japan; [7]Department of Surgery, University at Buffalo Jacobs School of Medicine and Biomedical Sciences, State University of New York, Buffalo, New York 14263, USA. [*]Equal contributors.

Received April 23, 2023; Accepted June 14, 2023; Epub July 15, 2023; Published July 30, 2023

Abstract: Autotaxin (ATX) is a secreted enzyme that produces extracellular lysophosphatidate in physiological wound healing. ATX is overexpressed in many cancers to promote growth, metastasis, and treatment resistance. However, ATX expression is very low in breast cancer cells, and is instead secreted by the tumor microenvironment (TME). Paracrine ATX expression, and its effects on tumor progression, has not been robustly studied in human breast tumors. In this study, ATX expression was analyzed in over 5000 non-metastatic breast cancers from databases TCGA, METABRIC and GSE96058, dichotomized by the median. Gene set enrichment analysis (GSEA) and the xCell algorithm investigated biological functions of ATX and correlation to TME cell populations. TME ATX production was verified by single cell RNA sequencing. The highest ATX expression occurred in endothelial cells and cancer-associated fibroblasts ($P<0.0001$). High tumor ATX expression correlated to increased adipocyte, fibroblast, and endothelial cell fractions ($P<0.01$), and GSEA demonstrated enriched immune system, tumor suppressor, pro-survival, stemness, and pro-inflammatory signaling in multiple gene sets. Tumor mutational burden was decreased, Ki67 scores were decreased, tumor infiltrating immune cell populations increased, and immune cytolytic activity scores increased (all $P<0.01$) for ATX-high tumors. Overall survival trends favored ATX-high tumors (hazard ratios 0.75-0.80). In summary, in human breast cancers, ATX is produced by the TME, and in non-metastatic tumors, high levels correlate with an anti-tumor phenotype. Because pre-clinical models use aggressive pro-metastatic cell lines where ATX-mediated signaling promotes tumorigenesis, further research is required to verify an anti-to-pro-tumor phenotype switch with breast cancer progression and/or treatment resistance.

Keywords: Adipose tissue, adjuvant therapy, cytokines, lysophosphatidic acid, novel therapeutics, tumor progression

Introduction

Breast cancer is the most common cancer in women with a 1 in 8 lifetime risk, accounting for just over 25% of all cancer diagnoses [1]. Five-year survival rates are about 99% when detected and treated as localized disease [2]. However, nearly 30% of breast cancers present with lymph node involvement and 6% with metastatic disease where the 5-year survival rates drop to 86% and 30%, respectively [2]. Nearly 300,000 women are diagnosed annually with breast cancer in the United States, and yet despite screening efforts and standard of care therapies, about 43,000 patients still die [3]. The majority of these deaths occur in women with relapsed disease that ultimately becomes resistant to treatment [4]. Understanding and

overcoming mechanisms of relapse and treatment failure are key areas of most modern breast cancer research [5].

Lysophosphatidate (LPA) is a potent extracellular bioactive signaling molecule that has been studied in pre-clinical cancer models for nearly 30 years [6, 7]. This lipid has multiple physiological roles related to proper embryogenesis and wound healing; however it can also act as a pathological mediator of chronic inflammation to promote cancer growth, survival against treatment, and metastasis [4, 7]. The majority of extracellular LPA is produced from biologically inert lysophosphatidylcholine (LPC) by the lysophospholipase D activity of the enzyme, ATX (gene name *ENPP2*) [8]. LPA signals through six G-protein coupled receptors to mediate its cellular effects [9]. LPA is broken down by the ecto-activity of the lipid phosphate phosphatases (LPPs) to monoacylglycerols (MAGs), which are mostly inactive signaling molecules [10]. Many cancer types, such as melanomas, thyroid cancers, and glioblastomas, overexpress ATX relative to normal tissue [7, 11]. In this setting, LPA signaling promotes chronic inflammation and decreased acquired immune responses, both of which are "hallmarks" of cancer [12, 13]. Chronic LPA signaling enables cancer cells to evade the immune system [11, 14], and increases vascular endothelial growth factor (VEGF) production and angiogenesis that is needed for tumor growth [15]. ATX expression correlates with tumor invasiveness [7, 16, 17], and in metastatic tumors, *ENPP2* is one of the 40-50 most up-regulated genes [18-20]. Breast cancer cells, however, express little ATX compared to tumor stroma and surrounding adipose tissue [4, 6]. Instead, tumor-promoting inflammation leads to increased ATX production in breast tissue by cytokine-induced mechanisms, and the subsequently increased paracrine ATX production increases the overall LPA concentrations in the tumor microenvironment [21, 22] (**Figure 1**). The overall effect is the establishment of a feedforward cycle that promotes a pro-cancer phenotype that upregulates resistance mechanisms against chemotherapy and radiotherapy regimens [6].

Inhibitors of LPA signaling, particularly ATX inhibitors, have been in pre-clinical and clinical trials for just over 10 years [23, 24]. As mitigators of chronic inflammation, the ATX inhibitor GLPG1690 (ziritaxestat) has progressed to Phase III clinical trials for the treatment of idiopathic pulmonary fibrosis [25, 26]. The ATX inhibitor, IOA-289, is now in a Phase 1b trial for pancreatic cancer (https://clinicaltrials.gov/ct2/show/NCT05586516). These, and other similar compounds, are synergistic in increasing the efficacy of chemotherapy and radiotherapy regimens against tumor growth and metastasis in immunocompetent models of murine triple negative breast cancer [21, 27-30]. However, while there are primarily immunohistochemical studies on human breast cancers that support the translation of our understanding of ATX signaling paradigms from pre-clinical models to patients [22, 31], the role of ATX in the human breast cancer tumor microenvironment has received relatively little attention.

In this study, we explore the role of ATX mRNA expression within the human breast cancer tumor microenvironment using *in silico* research methodologies. We examined the location of ATX expression by tumor cell populations using large databases of three independent cohorts. These were used to examine the effects of ATX expression in the tumor immune microenvironment and to survey ATX expression with respect to treatment effects and patient survival. We develop novel insights into the role of ATX signaling within human breast tumors, which will facilitate meaningful comparative analyses for pre-clinical studies to tailor the design of future pharmacological clinical studies.

Methods

Data acquisition

Clinical and mRNA expression breast cancer data from female patients were obtained from three databases: the Cancer Genome Atlas Program (TCGA) (whole database n = 1090, estrogen-receptor positive and human epidermal growth factor receptor negative tumors (ER+ HER2-) n = 593, HER2+ n = 184, triple negative breast cancer (TNBC) n = 160), the Molecular Taxonomy of Breast Cancer International Consortium (METABRIC) (whole database n = 1904, ER+ HER2- n = 1355, HER2+ n = 236, TNBC n = 313), and GSE96058 (whole database n = 3069, ER+ HER2- n = 2277, HER2+ n = 392, TNBC n = 155). TCGA and METABRIC results were obtained via the cBioPortal (https://www.cbioportal.org), and the expression data for TCGA was log-transformed using "data_mrna_seq_v2_rsem", while the METABRIC data was used as is with the "data_expression_median". GES96058 results were

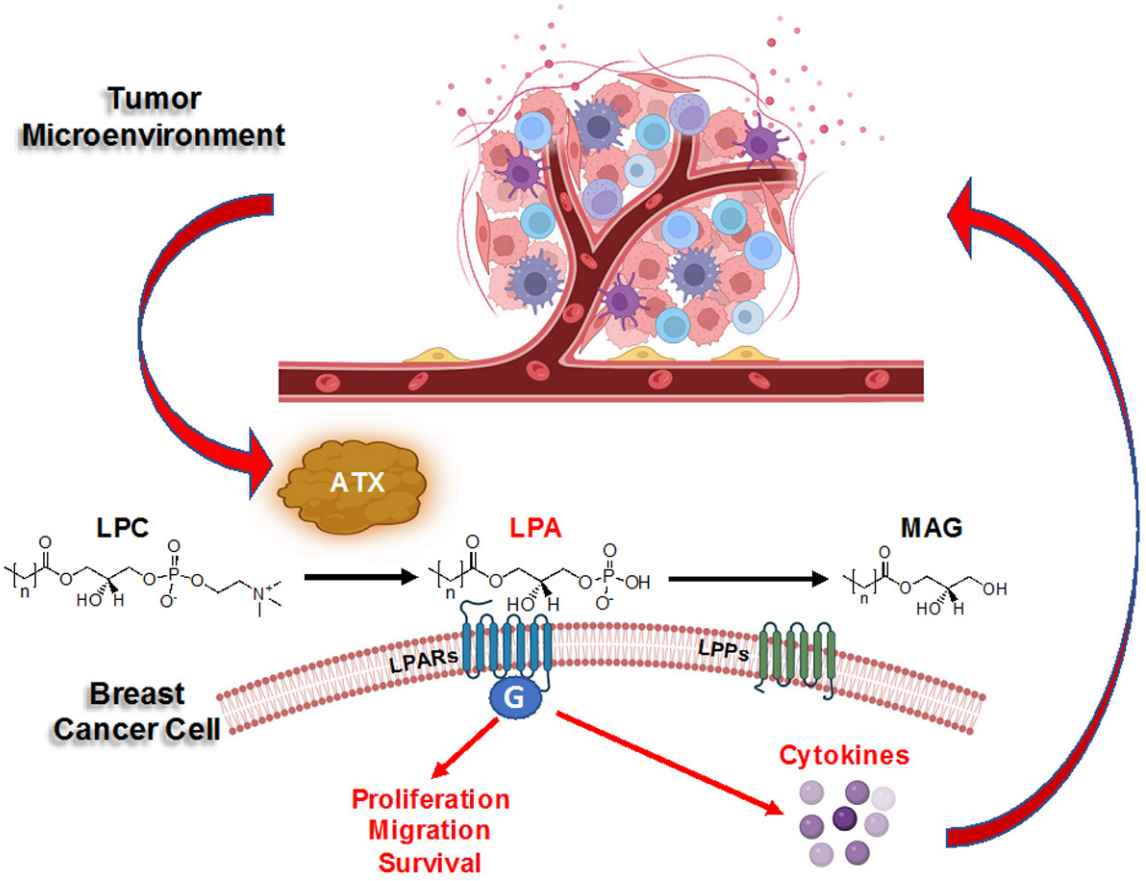

Figure 1. Overview of autotaxin (ATX) signaling in the breast cancer tumor microenvironment from pre-clinical studies. ATX is produced primarily by the breast cancer tumor stroma and surrounding inflamed adipose tissue in response to cytokines produced by the growing tumor. These cytokines in turn increase further production of ATX. The signaling effects of ATX are mediated by its production of extracellular lysophosphatidate (LPA) from lysophosphatidylcholine (LPC), which signals through six G-protein coupled receptors within the tumor to elicit pro-cancer effects. LPA is turned over to biologically inactive monoacylglycerol (MAG) by the ecto-activity of three enzymes known as the lipid phosphate phosphatases (LPPs).

downloaded from the Gene Expression Omnibus (GEO) repository of the United States National Institutes of Health (https://www.ncbi.nlm.nih.gov/geo), as described, and the provided normalized expression data from the database was used without any further processing [32, 33]. Gene expression data from 114 samples of normal breast tissue from female patients was obtained from the Genotype-Tissue Expression (GTex) Portal (https://gtexportal.org) [34].

Results from databases examining breast ATX expression from metastatic sites and in tumors before neoadjuvant therapy were also obtained from GEO. Several of these cohorts underwent annotation using the specified GPL for microarray datasets: GSE2034 (GPL96), GSE26388.1 (GPL1390), GSE26388.6 (GPL887), GSE25066 (GPL96), GSE20194 (GPL96), GSE20271 (GPL96), GSE22358 (GPL5325), GSE50948 (GPL570), GSE22226 (GPL1708), GSE34138 (GPL6884), GSE16446 (GPL570). In cases where multiple probes were assigned to *ENPP2*, the average value was employed. For the RNA sequencing datasets (GSE110590, GSE173661, GSE163882), the provided normalized expression data from the database was used without any further processing.

Single cell RNA sequencing breast cancer atlas data from female patients was also obtained for ATX expression from two large published cohorts [35, 36] via the Broad Institute Single Cell Portal (https://singlecell.broadinstitute.org/single_cell), using the accession numbers SCP1039 [35] and SCP1106 [36]. The downloaded features, matrix, and barcode data were integrated using the ReadMtx function in the Seurat package of R-4.2.1 (https://www.R-

project.org). Since the matrix data was already normalized at the time of download, no additional preprocessing or normalization steps were applied.

The total list of R packages used in data acquisition and processing is as follows: SeuratObject_4.1.3, Seurat_4.3.0, lubridate_1.9.2, forcats_1.0.0, dplyr_1.1.0, purrr_1.0.1, tidyr_1.3.0, tibble_3.1.8, tidyverse_2.0.0, SummarizedExperiment_1.28.0, GenomicRanges_1.49.0, GenomeInfoDb_1.34.3, IRanges_2.32.0, S4Vectors_0.36.0, MatrixGenerics_1.10.0, matrixStats_0.63.0, GEOquery_2.64.2, openxlsx_4.2.5.2, stringr_1.5.0, readxl_1.4.2, readr_2.1.4, Biobase_2.58.0, BiocGenerics_0.44.0, data.table_1.14.8, survminer_0.4.9, ggpubr_0.6.0, ggplot2_3.4.1, gtsummary_1.7.0, MASS_7.3-57, quantreg_5.94, SparseM_1.81, RcmdrMisc_2.7-2, sandwich_3.0-2, car_3.1-1, carData_3.0-5, backports_1.4.1, and survival_3.3-1.

Given that 99.4 percent of all breast cancer cases occur in females [37], and all databases used in the study contain only female patients, male breast cancer was not examined in this study. All data was downloaded in August 2022. Because all data was obtained from deidentified public databases or cohorts, ethics approval requirements were waived by the Roswell Park Institutional Review Board.

Gene set enrichment analysis (GSEA)

Functional enrichment analysis of *ENPP2* was performed by GSEA [38] on the Molecular Signatures Database Hallmark collection (http://www.gsea-msigdb.org) [39]. Gene sets with a false discovery rate (FDR) <0.25 specified enriched signaling [38]. High and low ATX expression groups were dichotomized by median gene expression. Positive NES scores indicate enriched signaling in the ATX-high expression group and negative NES scores indicate enriched signaling in the ATX-low expression group.

Other scores

The xCell algorithm (https://xcell.ucsf.edu) [40] was used to correlate ATX gene expression to the infiltrating fraction of TME stromal cells (adipocytes, preadipocytes, fibroblasts, endothelial cells, and pericytes), and immune cells (CD8+, T helper cell (Th)1 and Th2 cells, T-regulator cells, M1 and M2 macrophages, and dendritic cells) as described [41-44]. The mutational landscape of breast cancers (intratumor heterogeneity, homologous recombination defects, fraction genome altered, silent mutation rate, non-silent mutation rate, single-nucleotide neoantigens, and indel mutations), proliferation score, stromal fraction, TGF-β score, and immune scores (leukocyte fraction, lymphocyte infiltration, tumor infiltration lymphocyte fraction, macrophage regulation, and wound healing) were obtained from Thorsson *et al*. [45]. Immune cytolytic activity (CYT) in the TME was calculated as the geometric mean of the expression of perforin (*PRF1*) and granzyme A (*GZMA*) mRNA expression, which measures the anti-cancer ability of cytotoxic T cells [46].

Statistical analyses

Statistical analyses were conducted with R-4.2.1. Graphics were produced with the R software package and Origin Pro 2022 (OriginLab Corporation, Northampton, MA, USA). mRNA levels for *ENPP2* was dichotomized into low and high groups based on the median expression level. All results are plotted as box plots, with the lower and upper bounds representing the maximum and minimum values, the upper and lower ends of box representing the 25^{th} and 75^{th} percentile values and the bolded bar within the box representing the median value. For TCGA results (RNA sequencing data), units of expression are log2 transformed RSEM, METABRIC (microarray data), units of expression are log intensity levels, and all GSE results (RNA sequencing data) are log2 transformed CPM. Two group comparisons were performed using the Mann-Whitney U test and multiple group comparisons by the Kruskal-Wallis test. The R survival software package was used to analyze disease-free survival (DFS), disease-specific survival (DSS), and overall survival (OS) based on high or low ATX expression via Cox-proportional hazards regression. $P<0.05$ was set for statistical significance.

Results

High ATX expression may correlate to a more favorable breast cancer phenotype for non-metastatic tumors

We examined ATX expression levels by breast cancer characteristics. ATX expression tended

to be slightly higher for TNBCs than ER+ HER2- and HER2+ tumors, but this was not statistically significant in the GSE96058 cohort (**Figure 2**). There was no consistent trend across stages I-III (**Figure 2**). ATX expression negatively correlated with increasing grade in all three cohorts but was significant only in the TCGA and GSE96058 cohorts (**Figure 2**). There were no differences in ATX expression based on nodal status (**Figure 2**). There were only 29 metastatic tumors in both the TCGA and METABRIC cohorts, but overall, ATX levels were not different compared to non-metastatic tumors (**Figure 2**). In all three cohorts, increased ATX expression was negatively correlated to increasing Ki67 levels (**Figure 2**).

We additionally surveyed multiple other smaller cohorts reporting patient matched primary and metastatic breast tumors, however, ATX expression did not show any consistent trends across these studies (**Figure 3**). We also looked at the correlation between ATX expression before neoadjuvant chemotherapy and subsequent tumor response (pathological complete response or residual disease), but there were no significant differences (**Figure 4**).

We next examined survival trends based on median dichotomization between low and high ATX expression. Results are expressed as disease-free survival (DFS), disease-specific survival (DSS), and overall survival (OS). Overall, trends favored better survival for the high ATX expression tumors, but statistical significance was not achieved in all three cohorts. When examined by the entire cohort, high ATX expressing tumors had an OS hazard ratio (HR) of 0.75-0.80, and this result was statistically significant for the METABRIC and GSE96058 cohorts (**Figure 5**). These results were sub-analyzed by hormone type in **Figures 6**-**8**.

In many cancer subtypes, tumor mutational burden is a marker of cancer aggressiveness [47]. While intratumor heterogeneity was statistically similar, it trended lower in the high ATX expression group (**Figure 9**). Homologous recombination defects, fraction genome altered, silent mutation rates, and non-silent mutation rates were all significantly lower in the high ATX expression group (P<0.001) (**Figure 9**). Additionally, SNV neoantigen rates were significantly lower in high ATX expression tumors (P = 0.013), while indel mutations trended lower in this group (P = 0.29) (**Figure 9**).

ATX-mediated gene set enrichment patterns favor a pro-inflammatory and pro-survival phenotype

We next used gene set enrichment analysis (GSEA) on Hallmark pathways to investigate correlations to ATX gene expression [39]. Gene sets were selected that had significance across all three cohorts. The complete GSEA output is tabulated in Supplementary Table 1. Among the most enriched gene sets were the adipogenesis set with a normalized enrichment score (NES) between 1.5-2.2 (**Figure 10**). All other enriched gene sets can be grouped into five categories: immune system, tumor suppressor, survival, inflammatory, and stemness. Immune system gene sets were linked to allograft rejection, complement, and interferon-α and -γ responses (**Figure 10**). Tumor suppressor gene sets included apical surface and junction maintenance, apoptosis, and p53-mediated signaling. Survival gene sets included angiogenesis, hypoxia, reactive oxygen species (ROS) pathways, and xenobiotic metabolism. Inflammatory gene sets included the inflammatory response gene set, IL2-STAT5 and IL6-JAK-STAT3 signaling, TNF-α, and TGF-β. Stemness gene sets included the epithelial mesenchymal transition (EMT), Hedgehog signaling pathway, and KRAS. Most NES clustered between 1.4-1.9 for these gene sets (**Figure 10**).

ATX expression in human breast tumors is primarily in the tumor stroma

We examined ATX expression levels in breast tumors compared to normal breast tissue. ATX expression was about 1.16-fold higher in normal breast tissues compared to breast cancer tumors (P<0.001) (**Figure 11A**). We then examined two cohorts for which single cell RNA sequencing was performed on breast tumors. These both demonstrated that most ATX expression arose from endothelial cells and cancer-associated fibroblasts, followed by myeloid cell populations (**Figure 11B**, **11C**).

Additionally, we looked at scores by Thorsson *et al.* [45] related to tumor composition. ATX high tumors had lower proliferation scores (P<0.001), consistent with lower Ki67 scores in **Figure 2D** (**Figure 12A**). Instead, scores related to TGF-β response, a marker of stromal fibrosis, were significantly elevated (P<0.001, **Figure 12A**), and the overall stromal fraction increased from about 30 to 45% when comparing ATX low expression tumors to ATX high expression

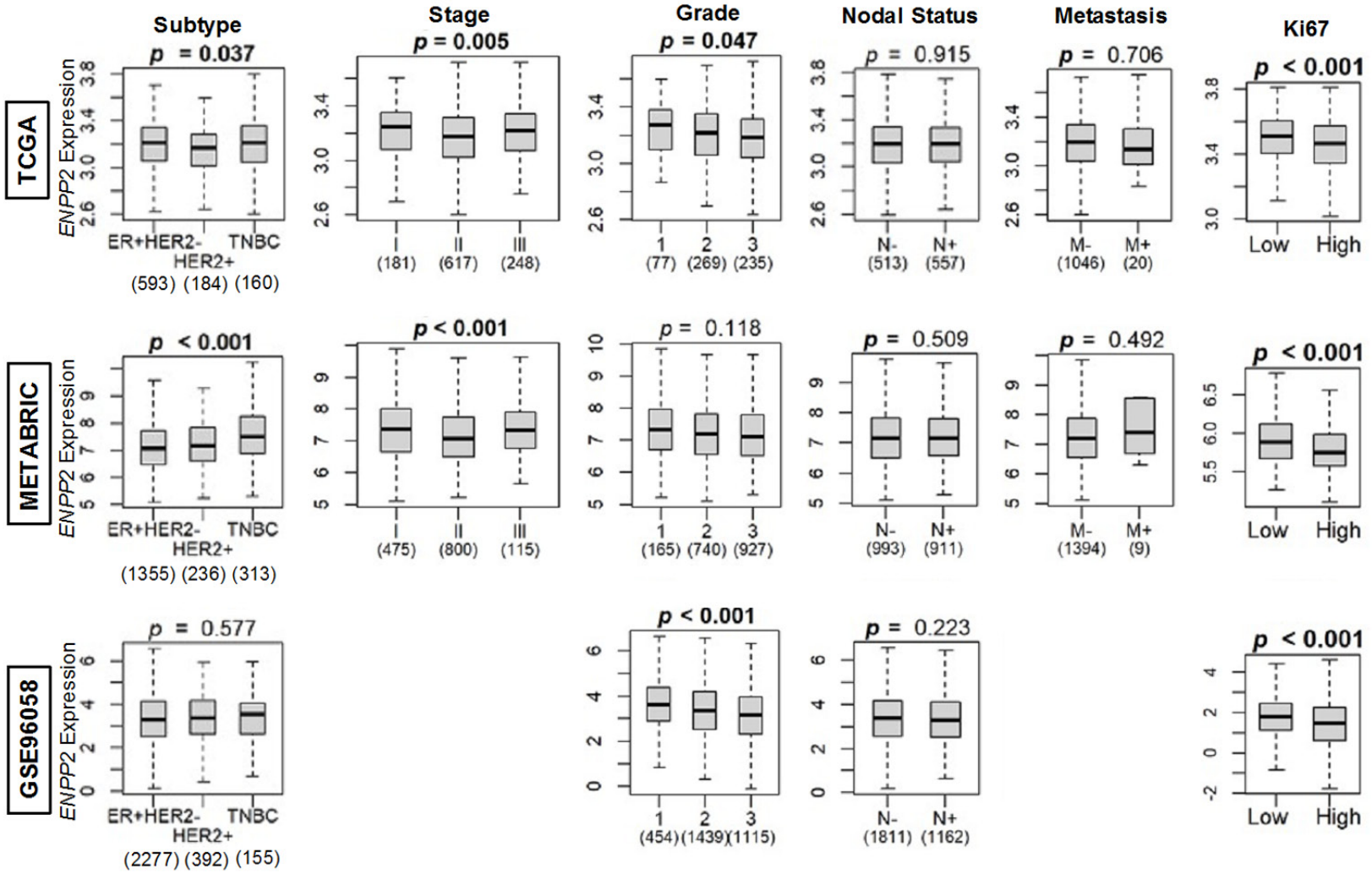

Figure 2. ATX (*ENPP2*) gene expression by breast cancer characteristics. Breast cancer subtype. ER+ HER2- (estrogen receptor positive, human epidermal growth factor receptor negative tumors), HER2+, TNBC (triple negative breast cancer). Staging according to the American Joint Committee on Cancer (AJCC). Stage is not available for the GSE96058 cohort. Grading according to AJCC. Tumor nodal status (negative or positive). Tumor metastasis (negative or positive). Because stage is not available for the GSE96058 cohort, metastasis data is also unavailable for this cohort. Ki67 box plots based on median *ENPP2* expression. Counts for non-median box plot groupings are displayed in brackets. Units of *ENPP2* expression: TCGA - log2 transformed RSEM, METABRIC - log intensity levels, and GSE96058 - log2 transformed CPM. The bolded center bar within the box plots represents the median, the lower and upper box bounds represent the 25th and 75th percentiles, respectively, and the lower and upper tails represent the minimum and maximum values, respectively.

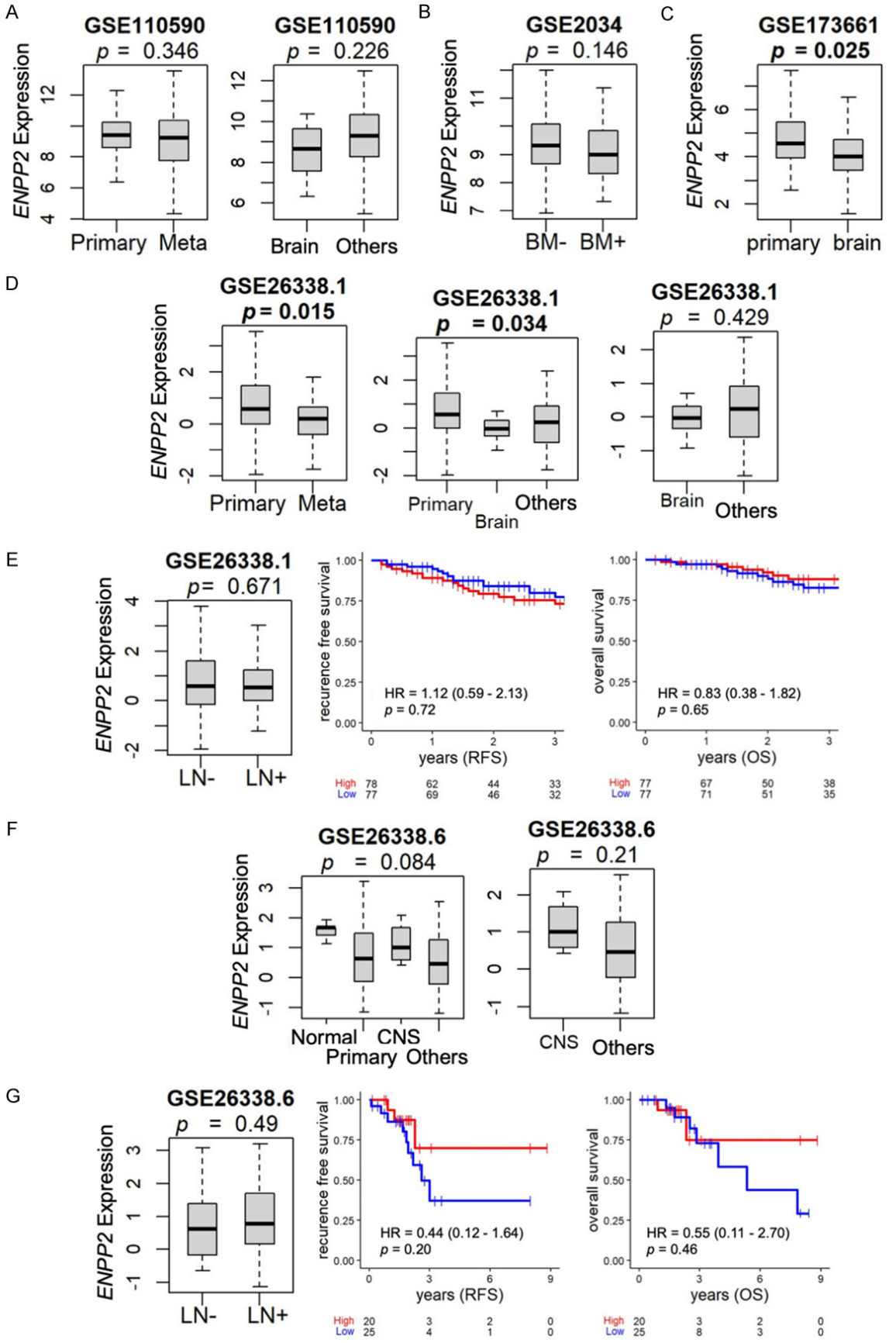
A
GSE110590
p = 0.346
ENPP2 Expression
Primary Meta
GSE110590
p = 0.226
Brain Others
B
GSE2034
p = 0.146
BM- BM+
C
GSE173661
p = 0.025
primary brain
D
GSE26338.1
p = 0.015
Primary Meta
GSE26338.1
p = 0.034
Primary Brain Others
GSE26338.1
p = 0.429
Brain Others
E
GSE26338.1
p = 0.671
LN- LN+
recurence free survival
HR = 1.12 (0.59 - 2.13)
p = 0.72
years (RFS)
overall survival
HR = 0.83 (0.38 - 1.82)
p = 0.65
years (OS)
F
GSE26338.6
p = 0.084
Normal CNS
Primary Others
GSE26338.6
p = 0.21
CNS Others
G
GSE26338.6
p = 0.49
LN- LN+
recurence free survival
HR = 0.44 (0.12 - 1.64)
p = 0.20
years (RFS)
overall survival
HR = 0.55 (0.11 - 2.70)
p = 0.46
years (OS)

Figure 3. ATX (*ENPP2*) expression and survival trends for locally advanced or metastatic breast cancer tumors. A. Results from 17 primary tumors (Primary) and 66 metastatic (Meta) tumors from matched patients (left), and comparison between 10 brain metastases (Brain) and 56 other non-brain specimens (Others) (right). B. Results from 217 primary tumors without bone metastasis (BM-) and 69 primary tumors with bone metastasis (BM+). C. Results from 45 primary tumors with patient matched brain metastasis tumors. D. Results from 204 primary tumors, from which patients a total of 29 metastasis occurred (left). ATX expression comparison among the 204 primary tumors, 8 brain metastatic tumors, and 21 metastatic tumors from non-brain sites (middle). Direct comparison between the 8 brain metastatic tumors and 21 metastatic tumors from non-brain sites (right). E. Results from 104 primary tumors without lymph node (LN) involvement, and 75 with LN involvement (left). Recurrence free survival (middle) and overall survival (right) dichotomized by medial ATX expression for this cohort. F. Results from 5 normal breast tissues (Normal), 71 primary tumors (Primary), 4 central nervous system (CNS) metastatic tumors, and 20 metastatic tumors at other sites (Other) (right). Comparison between the CNS and other sites (left). G. Results from 36 primary tumors without LN involvement, and 33 with LN involvement (left). Recurrence free survival (middle) and overall survival (right) dichotomized by medial ATX expression for this cohort. All units of *ENPP2* expression are log2 transformed CPM.

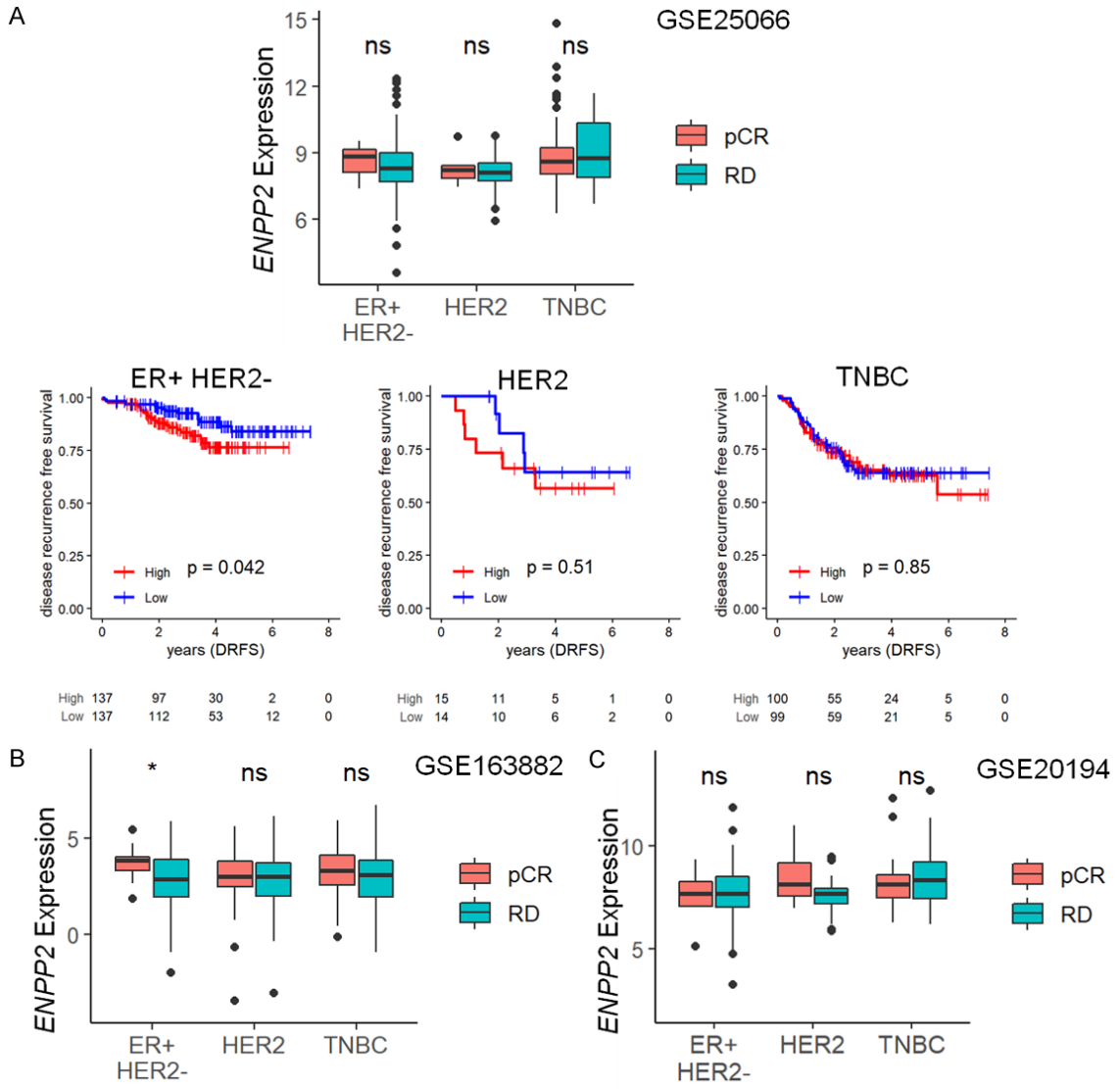

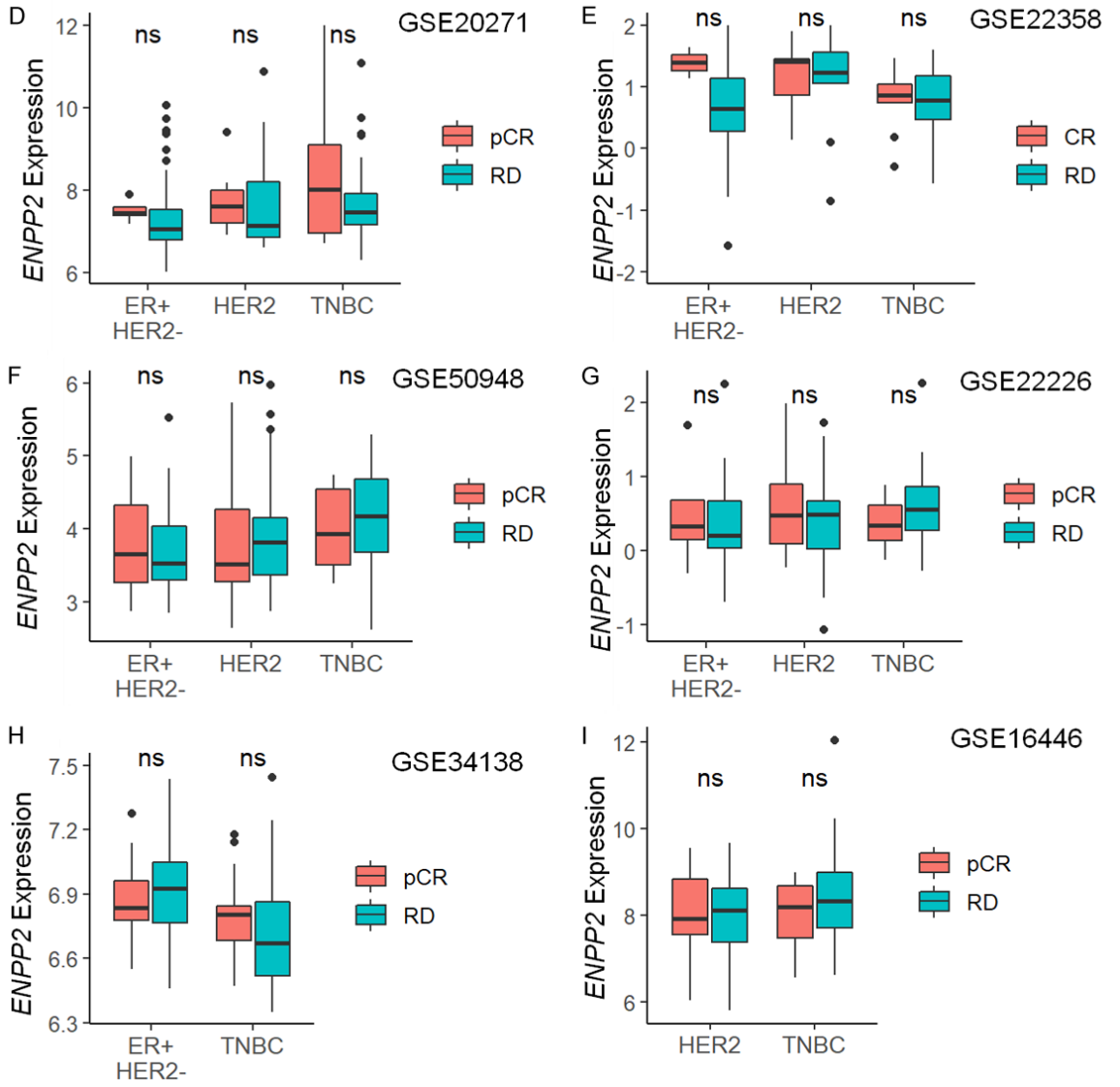

Figure 4. Association between neoadjuvant chemotherapy (NAC) response (pathological complete response (pCR) and residual disease (RD)) and ATX (*ENPP2*) expression levels from pre-treatment biopsies. A. NAC regimen: AC-T (doxorubicin and cyclophosphamide followed by paclitaxel); ER+ HER2- n = 274, HER2 n = 29, TNBC n = 199. Disease recurrence free survival plots for the entire cohort dichotomized into low and high ATX expression by the mean are shown for each hormonal subtype. B. NAC regimen: anthracycline and taxane (± trastuzumab); ER+ HER2- n = 69, HER2 n = 63, TNBC n = 90. C. NAC regimen: TFAC (paclitaxel, 5-fluorouracil, doxorubicin, cyclophosphamide); ER+ HER2- n = 140, HER2 n = 59, TNBC n = 79. D. NAC regimen: FAC/TFAC; ER+ HER2- n = 89, HER2 n = 26, TNBC n = 63. E. NAC regimen: Docetaxel and capecitabine; ER+ HER2- n = 67, HER2 n = 34, TNBC n = 52. F. NAC regimen: AT followed by CMF (cyclophosphamide, methotrexate, 5-fluorouracil), or the same regimen in combination with trastuzumab for 1 year; ER+ HER2- n = 25, HER2 n = 114, TNBC n = 17. G. NAC regimen: AC-T; ER+ HER2- n = 41, HER2 n = 39, TNBC n = 31. H. NAC regimen: dose-dense doxorubicin and cyclophosphamide; ER+ HER2- n = 119, TNBC n = 57. I. NAC regimen: Anthracycline (epirubicin) monotherapy; HER2 n = 31, TNBC n = 62. The bolded center bar within the box plots represents the median, the lower and upper box bounds represent the 25th and 75th percentiles, respectively, and the lower and upper tails represent the 1 percentile and 99 percentile values, respectively, with black dots representing values outside these percentiles. All units of *ENPP2* expression are log2 transformed CPM. ER, estrogen receptor; HER2, human epidermal growth factor receptor; NAC, neoadjuvant chemotherapy; NS, not significant; TNBC, triple negative breast cancer.

tumors (P<0.001, **Figure 12A**). We then used the xCell algorithm to examine estimates of tumor cell populations based on dichotomized ATX expression. Epithelial cells, representative of cancer cells, did not demonstrate consistent differences between high and low ATX

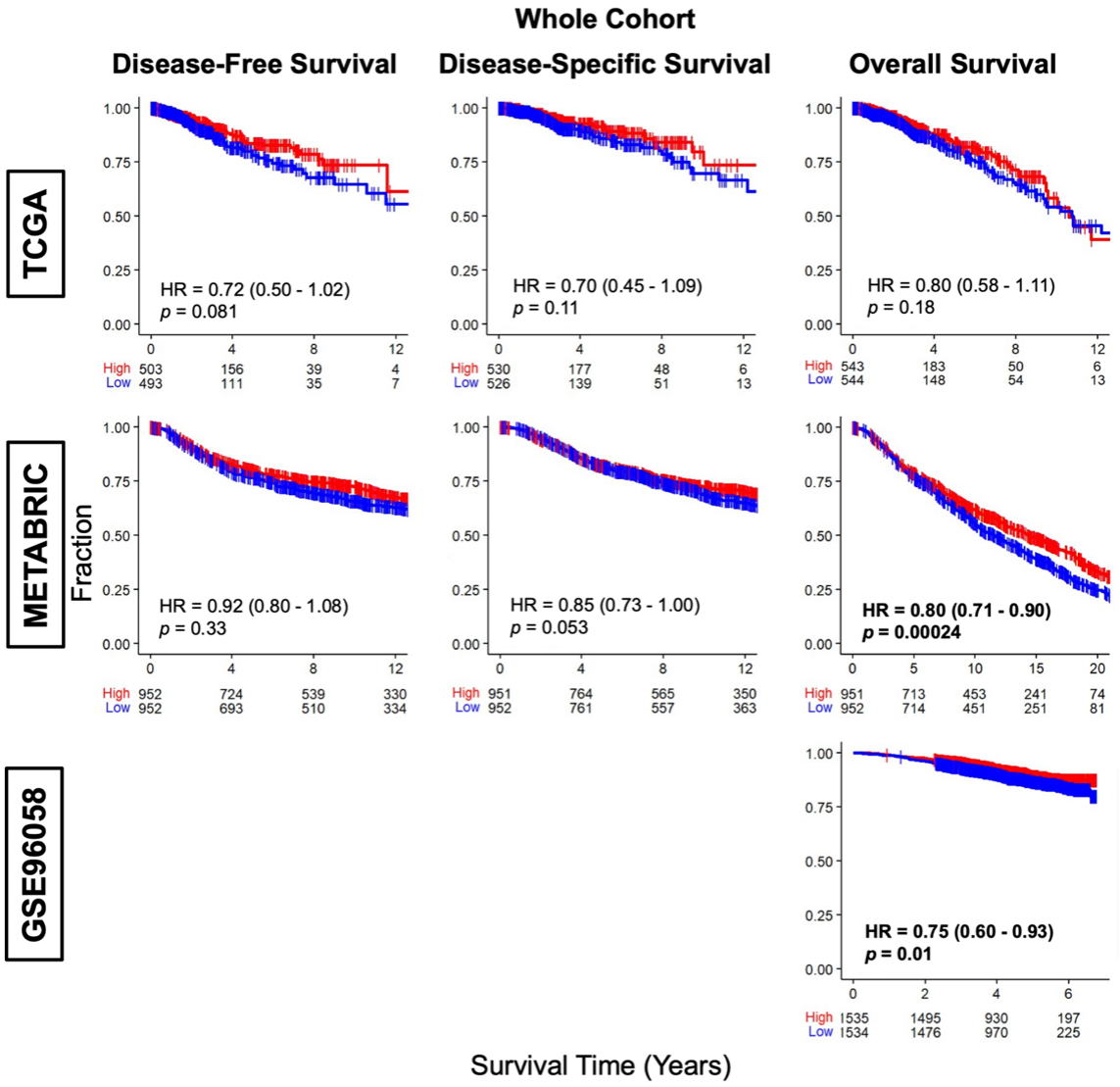

Figure 5. Survival plots for low and high ATX (*ENPP2*) gene expression in breast tumors for the whole cohort for each dataset. Patients at risk for each time point are listed along the x-axis. *ENPP2* expression is dichotomized into low and high groups by the median. The hazard ratio (HR) compares the high group against the low group.

expression groups, but tended to have lower epithelial cell composition in ATX-high tumors in the METABRIC and GSE96058 cohorts (both $P<0.001$, **Figure 12B**). This is consistent with decreased ATX in tumors in **Figure 11A**, and decreased proliferation scores in **Figure 12A**. Conversely, fibroblasts, adipocytes, and preadipocyte compositions were all significantly increased in all three cohorts in ATX-high tumors compared to ATX-low tumors (all $P<0.001$, **Figure 12B**).

Because endothelial cells were high expressors of ATX in single cell RNA sequencing (**Figure 11B**, **11C**), we also examined endothelial cells via the xCell platform. Across all three cohorts, endothelial cells, microvascular endothelial cells, and lymphatic endothelial cells were significantly enriched in ATX-high tumors compared to ATX-low tumors (all $P<0.01$, **Figure 13**). Pericyte populations were additionally examined; however, there was not a consistent trend across the three cohorts for the ATX-high tumors (elevated in TCGA, decreased in METABRIC, and no difference in GSE96058) (**Figure 13**).

High ATX expression in breast tumors correlates to an overall increased immune cell population in the tumor microenvironment

We next examined the correlation between immune cell populations and ATX expression

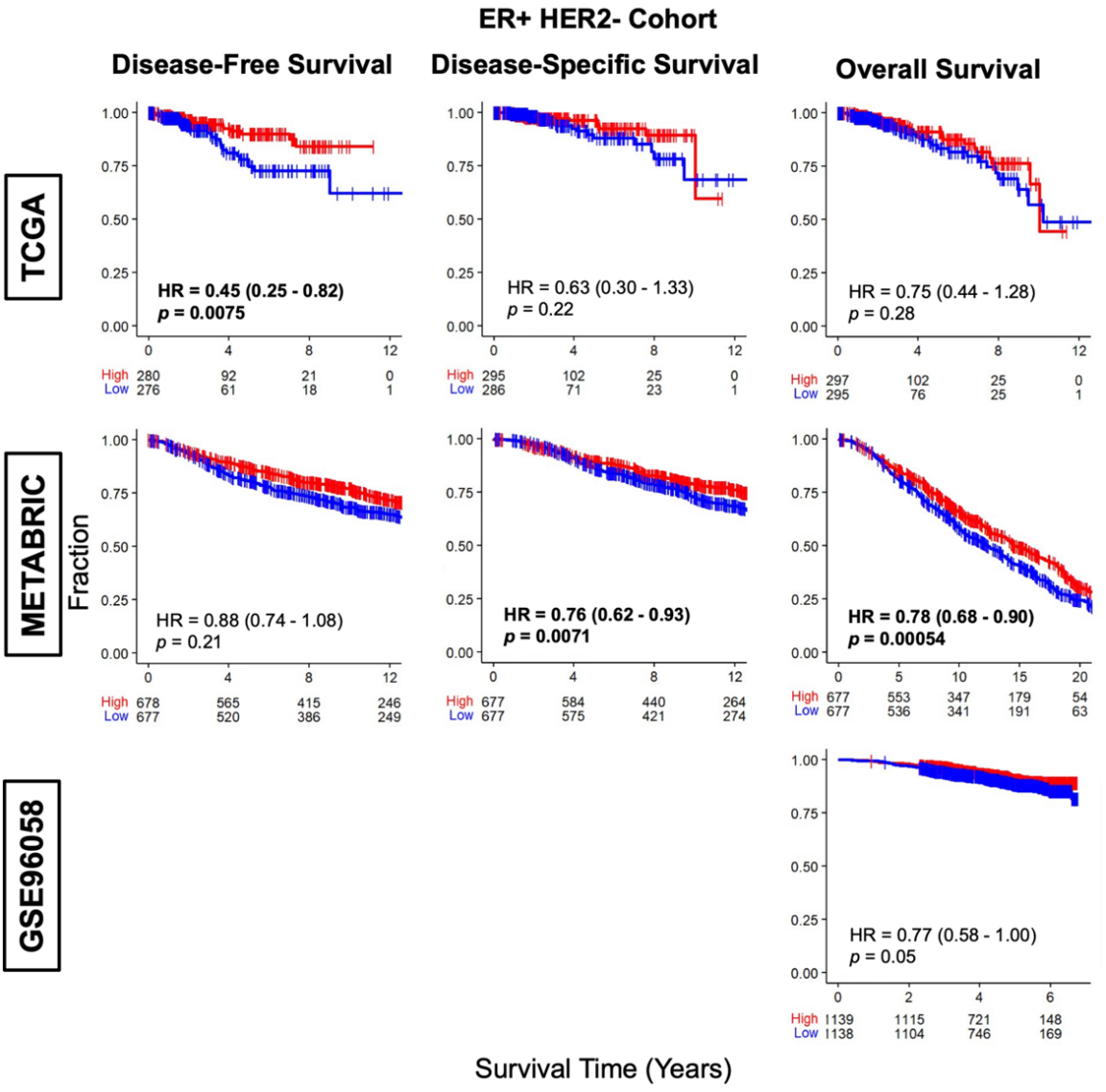

Figure 6. Survival plots for low and high ATX (*ENPP2*) gene expression in breast tumors for the estrogen receptor (ER)-positive, human epidermal growth factor receptor (HER2)-negative cohort for each dataset. Patients at risk for each time point are listed along the x-axis. *ENPP2* expression is dichotomized into low and high groups by the median. The hazard ratio (HR) compares the high group against the low group.

levels. Among the anti-cancerous immune cells, CD8+ T cells and dendritic cells were significantly elevated in high ATX expression tumors over low ATX expression tumors in all three cohorts (all $P<0.001$, **Figure 14A**). However, Th1 cells were decreased in all three cohorts in the high ATX expression tumors (all $P<0.001$), and there was no consistent trend for M1 macrophages (**Figure 14A**). For the pro-cancerous immune cell populations examined (Tregs, Th2 cells, and M2 macrophages), there was a lack of both significance and/or trend across the three cohorts, such that no conclusion could be made on their correlation to ATX expression levels (**Figure 14B**). On examination of immune related scores by Thorsson *et al.* [45], leukocyte fraction, lymphocyte infiltration, and macrophage regulation scores were all significantly increased in ATX-high tumors (**Figure 15A**). There was no difference in the tumor infiltrating lymphocyte (TIL) fraction between the two groups, while the wound healing score was decreased in the ATX-high tumor group ($P<0.001$, **Figure 15A**). Cytolytic (CYT)

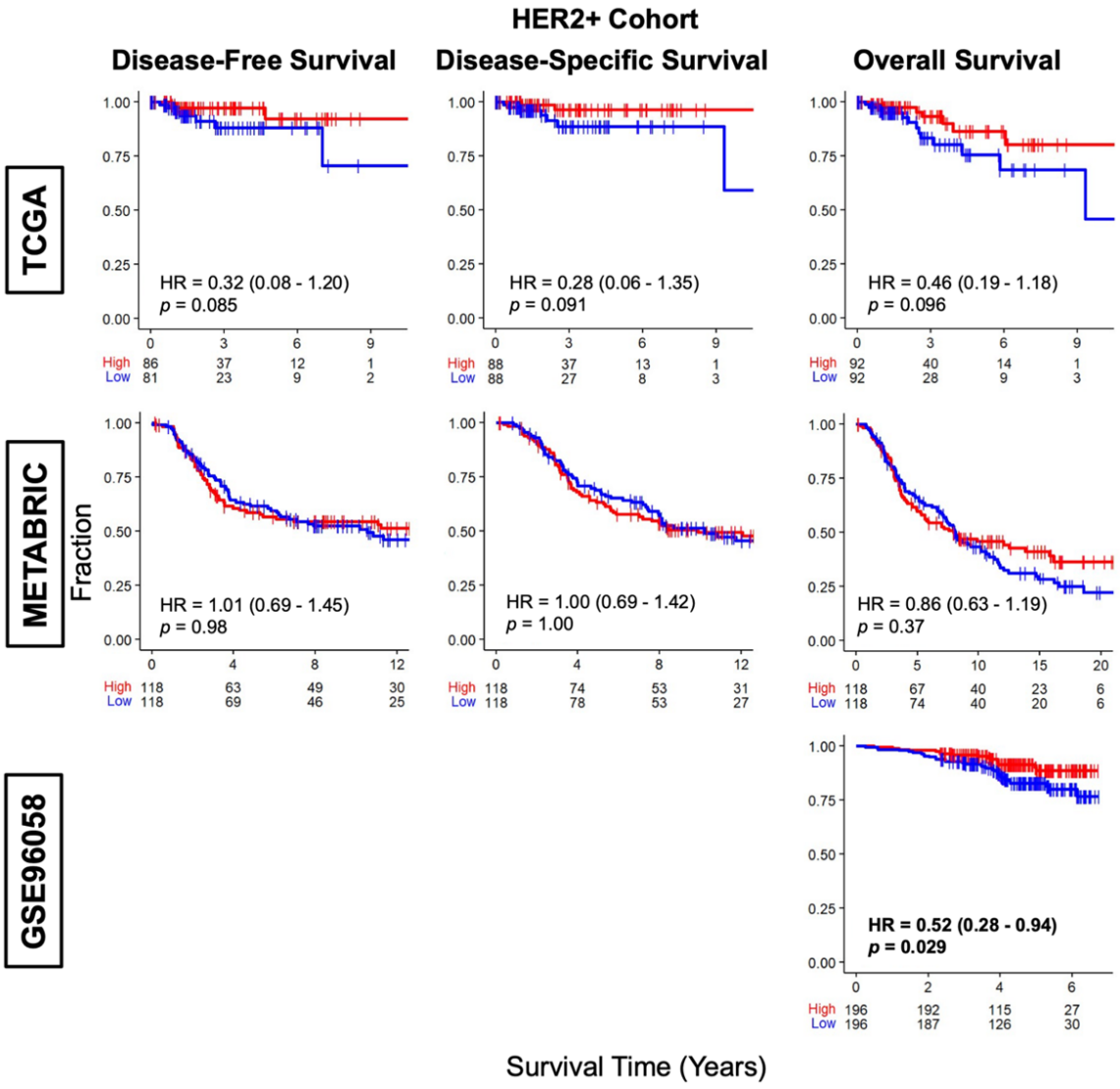

Figure 7. Survival plots for low and high ATX (*ENPP2*) gene expression in breast tumors for the human epidermal growth factor receptor (HER2)-positive cohort for each dataset. Patients at risk for each time point are listed along the x-axis. *ENPP2* expression is dichotomized into low and high groups by the median. The hazard ratio (HR) compares the high group against the low group.

scores were also significantly increased in all cohorts in the ATX-high tumor group ($P<0.001$, **Figure 15B**).

Correlation patterns between ATX and LPA receptors (LPARs) and the lipid phosphate phosphatases (LPPs)

Lastly, we examined the correlation between ATX expression and the LPARs and LPPs. High ATX expression tumors also had increased *LPAR1, 3, 4, 6* expression compared to low ATX expression tumors in all three cohorts (all $P<0.001$, **Figure 16A**). *LPAR2* expression was slightly decreased in high ATX expression tumors ($P\leq0.05$), and no consistent trends were seen for *LPAR5* (**Figure 16A**). For the LPPs, LPP1 and 3 gene expression was significantly increased and LPP2 gene expression was decreased in all three cohorts in high ATX expression tumors (all $P<0.001$, **Figure 16B**).

Discussion

ATX was first identified in melanoma cell culture in 1992 as an “autocrine motility factor”, but it would take another ten years before it was realized that ATX exerted its effects through its

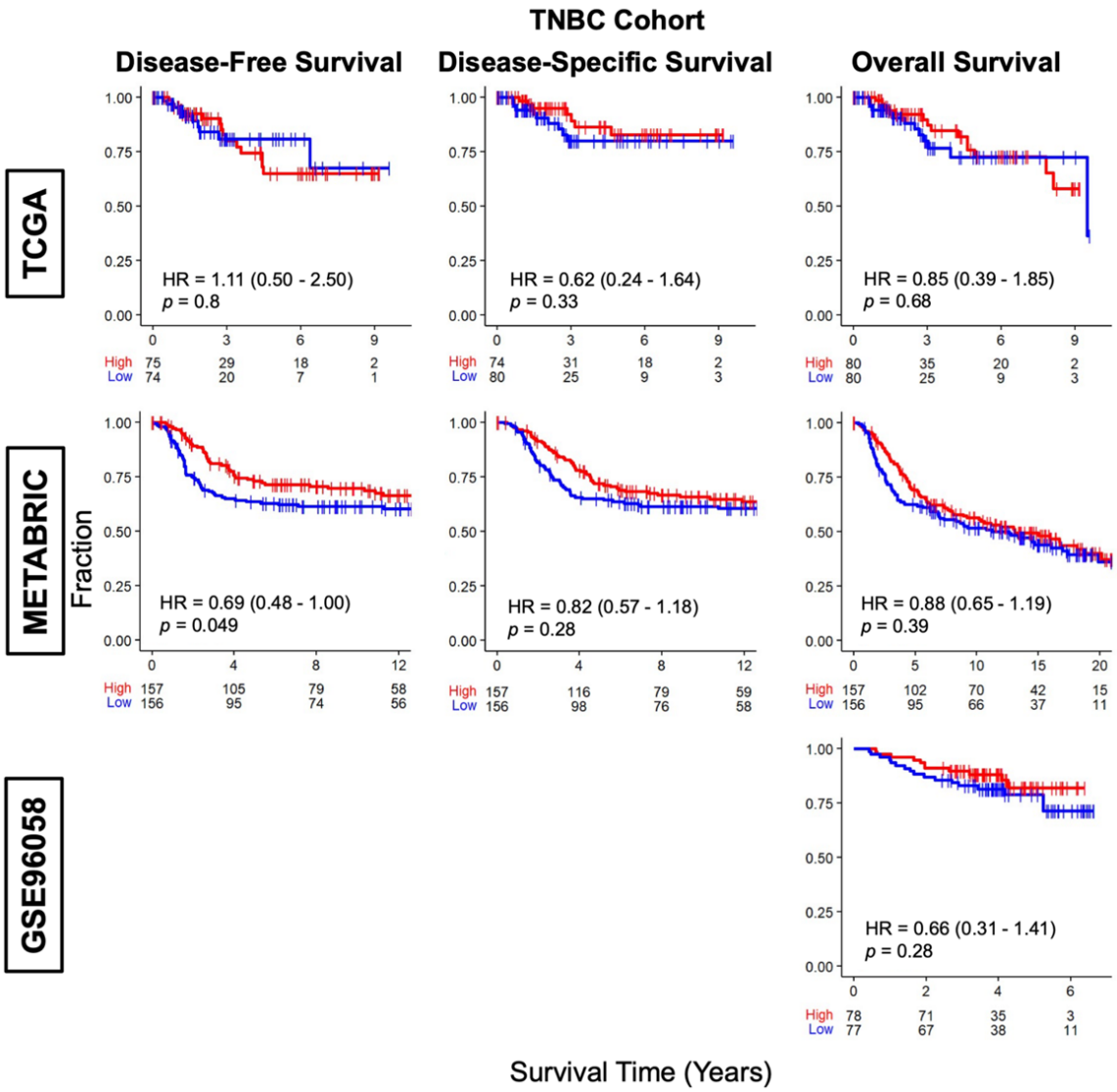

Figure 8. Survival plots for low and high ATX (*ENPP2*) gene expression in breast tumors for the triple negative breast cancer (TNBC) cohort for each dataset. Patients at risk for each time point are listed along the x-axis. *ENPP2* expression is dichotomized into low and high groups by the median. The hazard ratio (HR) compares the high group against the low group.

plasma lysophosphatase D activity via conversion of LPC to LPA [48-50]. Shortly thereafter, initial breast cancer studies *in vitro* showed transfection of ATX into breast cancer cells increased motility and invasiveness [51, 52], and LPA signaling protected breast cancer cell lines from chemotherapy-induced apoptosis [53, 54]. A seminal paper in 2009 then demonstrated that mammary mouse tumor virus (MMTV) mice, which overexpressed ATX or LPAR1, 2, or 3 had higher rates of breast tumorigenesis and metastasis [55]. Around this same time in the late 2000s/early 2010s, ATX was shown to be physiologically vital for proper embryogenesis because ATX knockout in mice was embryonically lethal at day 9.5 secondary to vascular and neural tube defects [56, 57]. In the post-natal organism, ATX/LPA signaling is vital for wound healing and tissue remodeling via platelet aggregation, and the growth and migration of fibroblasts, vascular smooth muscle cells, endothelial cells, and keratinocytes [7, 58]. From these discoveries, the ATX field naturally translated to chronic inflammation as a promoter of the cancer phenotype [59, 60].

Nearly ten years ago, we showed that breast cancer cells are very poor expressers of ATX

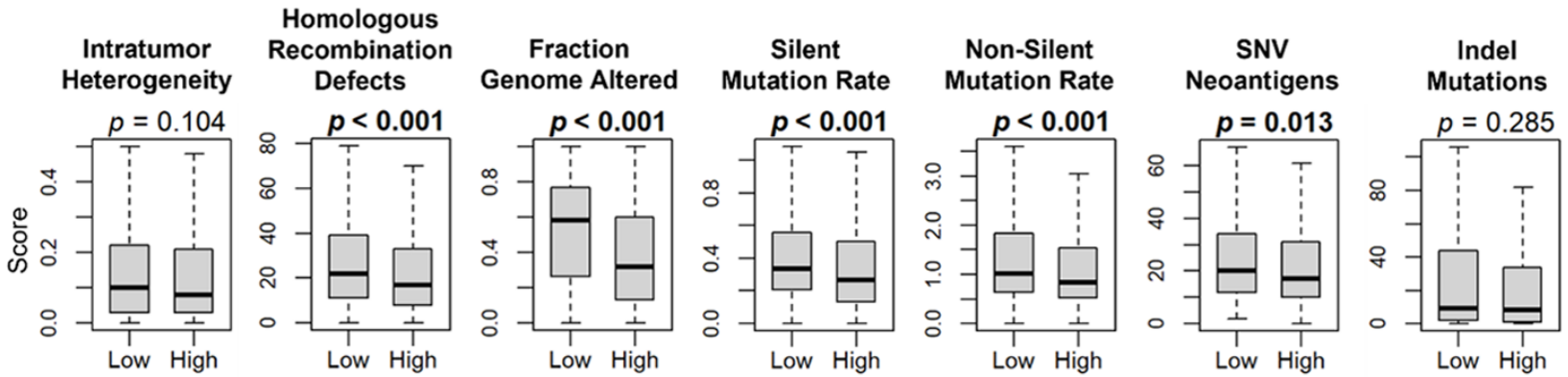

Figure 9. ATX (*ENPP2*) gene expression association with breast cancer mutations. Box plots of intratumor heterogeneity, homologous recombination defects, fraction genome altered, silent mutation rate, non-silent mutation rate, single-nucleotide variant (SNV) neoantigens, and indel mutations. Data is based on the scores by Thorsson *et al.* [45]. *ENPP2* expression is dichotomized into low and high groups by the median (total counts by cohort: TCGA - 1090, METABRIC - 1094, GSE96058 - 3609). Units of *ENPP2* expression: TCGA - log2 transformed RSEM, METABRIC - log intensity levels, and GSE96058 - log2 transformed CPM. The bolded center bar represents the median, the lower and upper box bounds represent the 25th and 75th percentiles, respectively, and the lower and upper tails represent the minimum and maximum values, respectively.

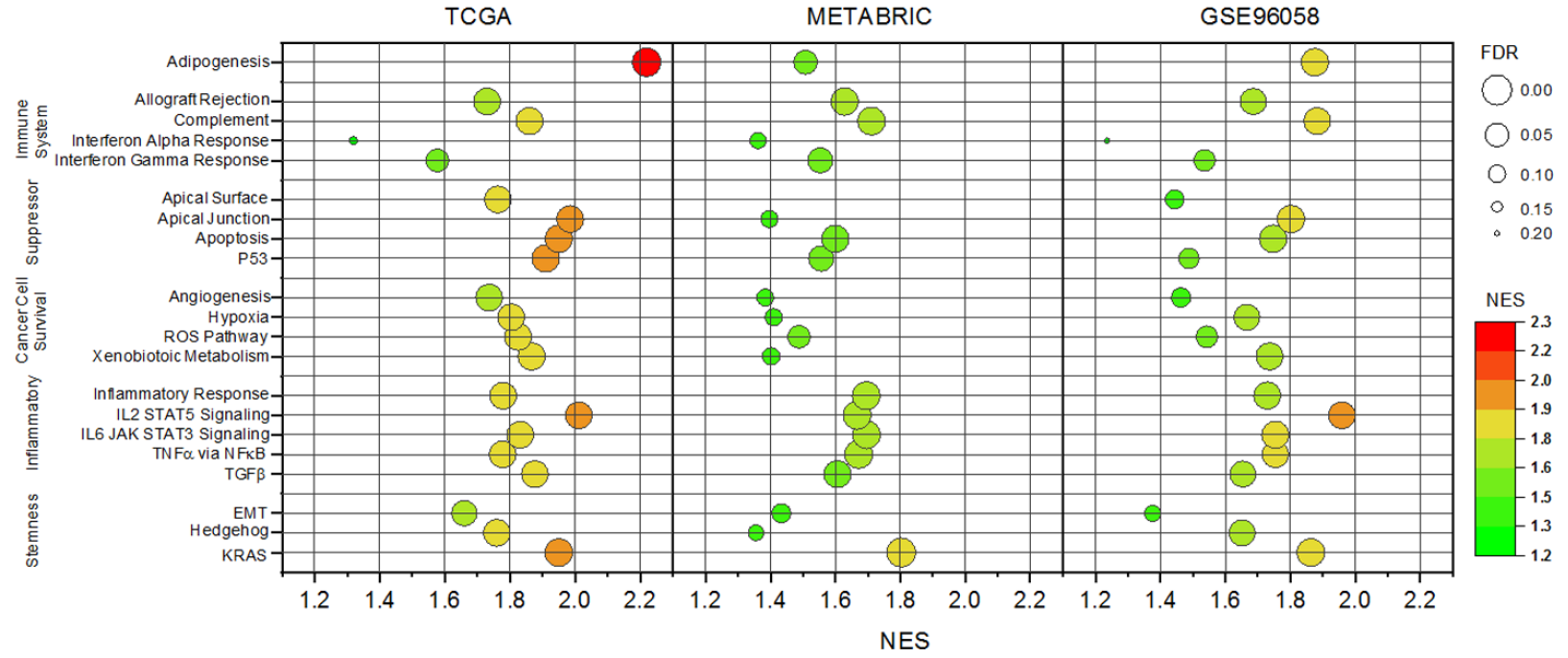

Figure 10. Gene set enrichment analysis (GSEA) for ATX (*ENPP2*) in breast cancer. Gene sets are grouped into common themes. All gene sets displayed were significantly increased in all three datasets examined. A false discovery rate (FDR) of less than 0.25 was considered statistically significant. Dot size represents the FDR value, and they are colored according to the normalized enrichment score (NES).

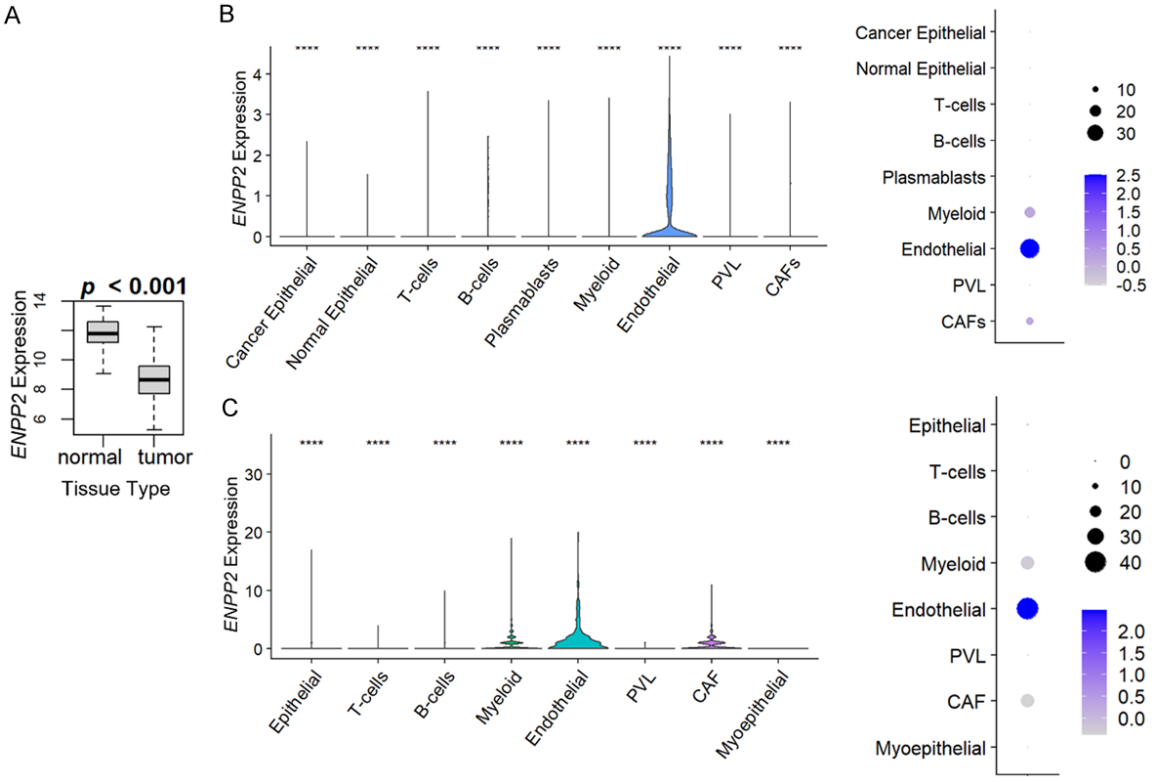

Figure 11. ATX gene expression (*ENPP2*) is increased in normal breast tissue compared to breast cancer tumors and is primarily produced by tumor stromal cells. (A) mRNA expression from 114 normal breast tissues is compared to 1090 breast cancer tumors from the TCGA database. Results are plotted as box plots. The bolded center bar represents the median, the lower and upper box bounds represent the 25th and 75th percentiles, respectively, and the lower and upper tails represent the minimum and maximum values, respectively. (B) Results from cohort described in [36], comprised of 26 tumors (11 ER+ HER2-, 5 HER2+, and 10 TNBC), with a total of 130,246 single cells. (C) Results from cohort described in [35], comprised of 5 TNBC tumors, with a total of 24,271 single cells. For results in (B, C), violin plot results are shown following *t*-test for each type compared with the base mean (****P≤0.0001). The summary chart shows the overall percentage of the total ATX expression by cell type and the average expression within each cell type for each cohort.

relative to normal breast tissue. We demonstrated using an immunocompetent orthotopic Balb/c/4T1 mouse model of triple negative breast cancer, that the growing breast tumor induces ATX expression and enzyme production in surrounding breast adipose tissue through the secretion of multiple inflammatory cytokines [21, 22]. This increased ATX/LPA signaling in turn increased cancer cell cytokine production, establishing a feedforward inflammatory cycle [21, 22]. Treatment with an oral ATX inhibitor slowed tumor growth and metastasis [21], and was synergistic with both conventional chemotherapy [27-29], and radiotherapy [30, 61, 62]. We also showed that LPA, through feedback inhibition, can inhibit ATX transcription, but this inhibition can be overcome with cancer-induced cytokine production, particularly in advanced pre-clinical models of breast tumors [63]. We further demonstrated that this pattern of cytokine-induced ATX production also occurs in human breast tumors through immunohistochemical studies where cytokines increase ATX staining in tumor adjacent stroma compared to more distant stroma [4, 22].

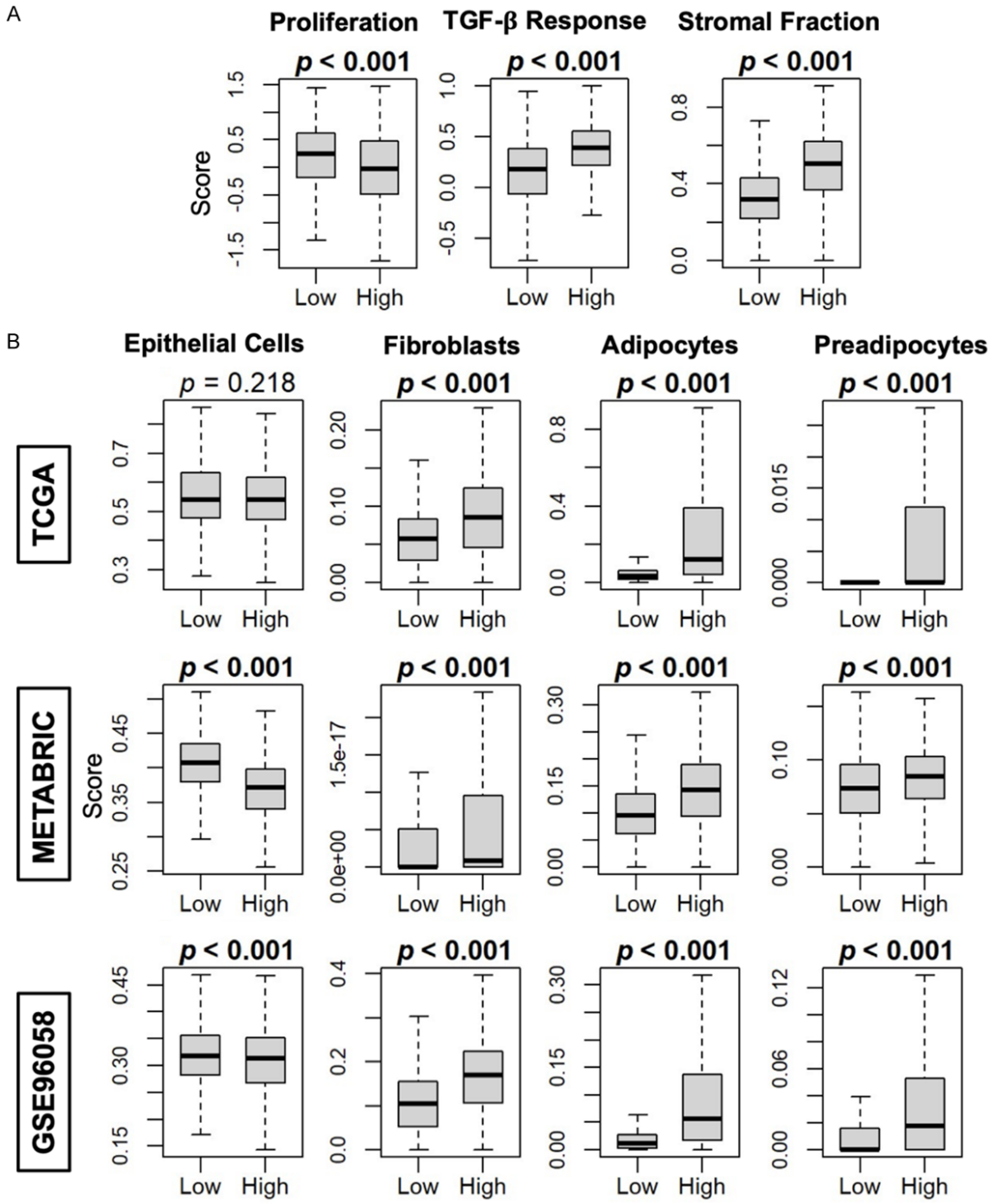

Figure 12. Proliferation and stromal related scores, and epithelial, fibroblast, adipocyte, and preadipocyte composition correlation with ATX (*ENPP2*) expression in breast cancer. A. Box plots of calculated scores for proliferation, TGF-β response, and stromal fraction based on Thorsson *et al.* [45]. B. Box plots of epithelial cell, fibroblast, adipocyte, and preadipocyte composition based on the xCell algorithm for the TCGA, METABRIC, and GSE96058 cohorts. *ENPP2* expression is dichotomized into low and high groups by the median (total counts by cohort: TCGA - 1090, METABRIC - 1094, GSE96058 - 3609). The bolded center bar represents the median, the lower and upper box bounds represent the 25th and 75th percentiles, respectively, and the lower and upper tails represent the minimum and maximum values, respectively.

In recent years, there is growing interest in exploring the effects of DNA methylation on ATX expression in breast tissue, and its influence on tumor biology [64]. *ENPP2* has been found

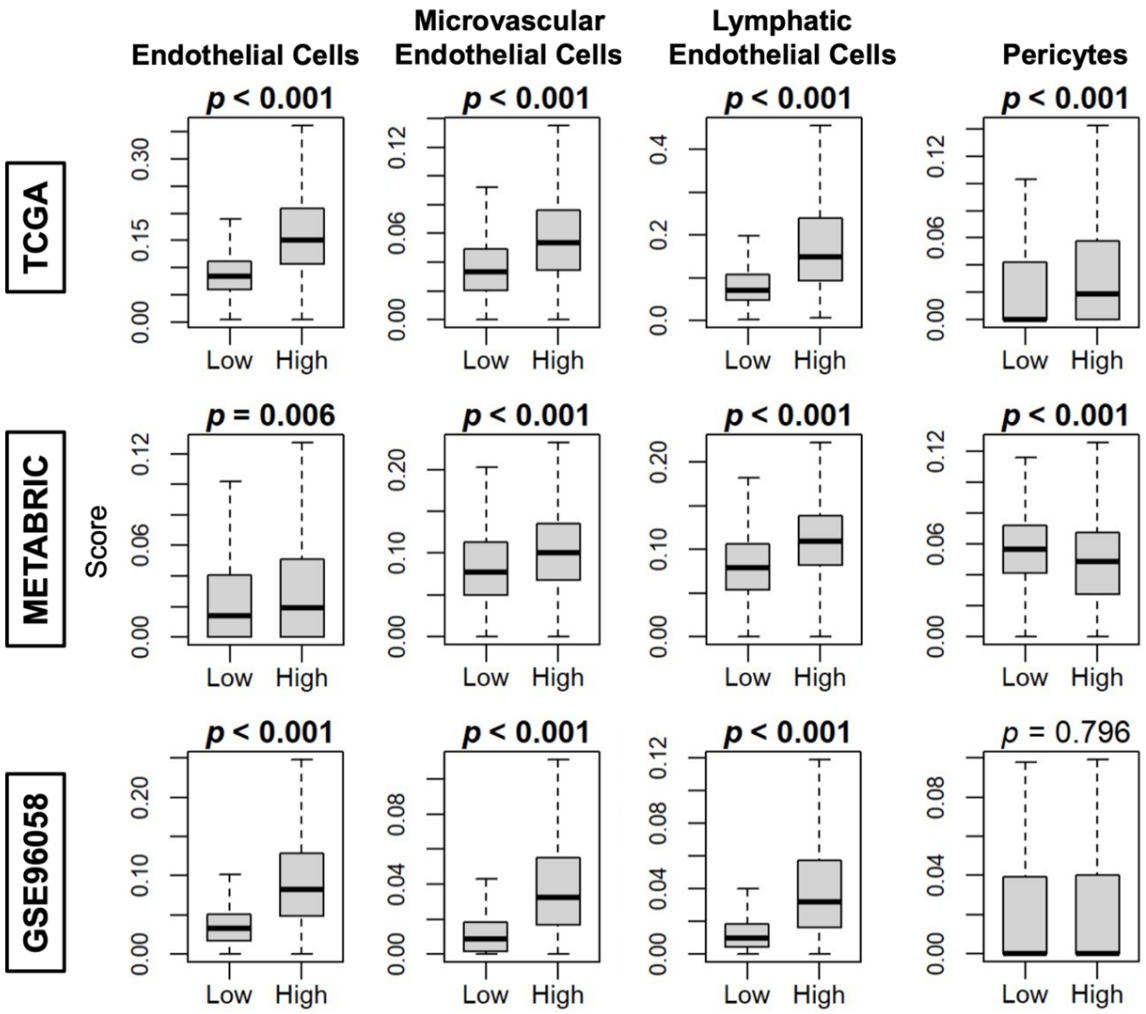

Figure 13. Endothelial cell, microvascular endothelial cell, lymphatic endothelial cell, and pericyte composition correlation with ATX (*ENPP2*) expression in breast cancer. Box plots of endothelial cell, microvascular endothelial cell, lymphatic endothelial cell, and pericyte composition based on the xCell algorithm for the TCGA, METABRIC, and GSE96058 cohorts. *ENPP2* expression is dichotomized into low and high groups by the median (total counts by cohort: TCGA - 1090, METABRIC - 1094, GSE96058 - 3609). The bolded center bar represents the median, the lower and upper box bounds represent the 25th and 75th percentiles, respectively, and the lower and upper tails represent the minimum and maximum values, respectively.

to be highly methylated in breast cancer tissues, and some work has shown *ENPP2* hypermethylation to correlate to disease progression [65]. Studies though that have examined ATX expression and subsequent protein expression in human breast tumors have been few to date. Among the first was an immunohistochemical study that showed stromal ATX was upregulated in 50% of stage III and IV breast cancers (6/12 specimens), as opposed to 17.6% of stage II cancers (3/17 specimens), and 0% of stage I cancers (0/15 specimens) [31]. Another study comparing serum ATX levels in 112 patients with breast cancer compared to 50 healthy patients showed that ATX levels were higher in breast cancer patients, and increased significantly in a stepwise fashion with increasing clinical stage of disease [66]. However, because ATX is a soluble ecto-enzyme, immunohistochemistry results do not indicate which cells in the tumor microenvironment produce the ATX. When trying to correlate these immunohistochemistry findings to those that demonstrate hypermethylation with disease progression, the logical conclusion is that as tumors progress, they rely increasingly heavily on the ATX produced by tumor surrounding stroma or host tissues including platelets [4, 66].

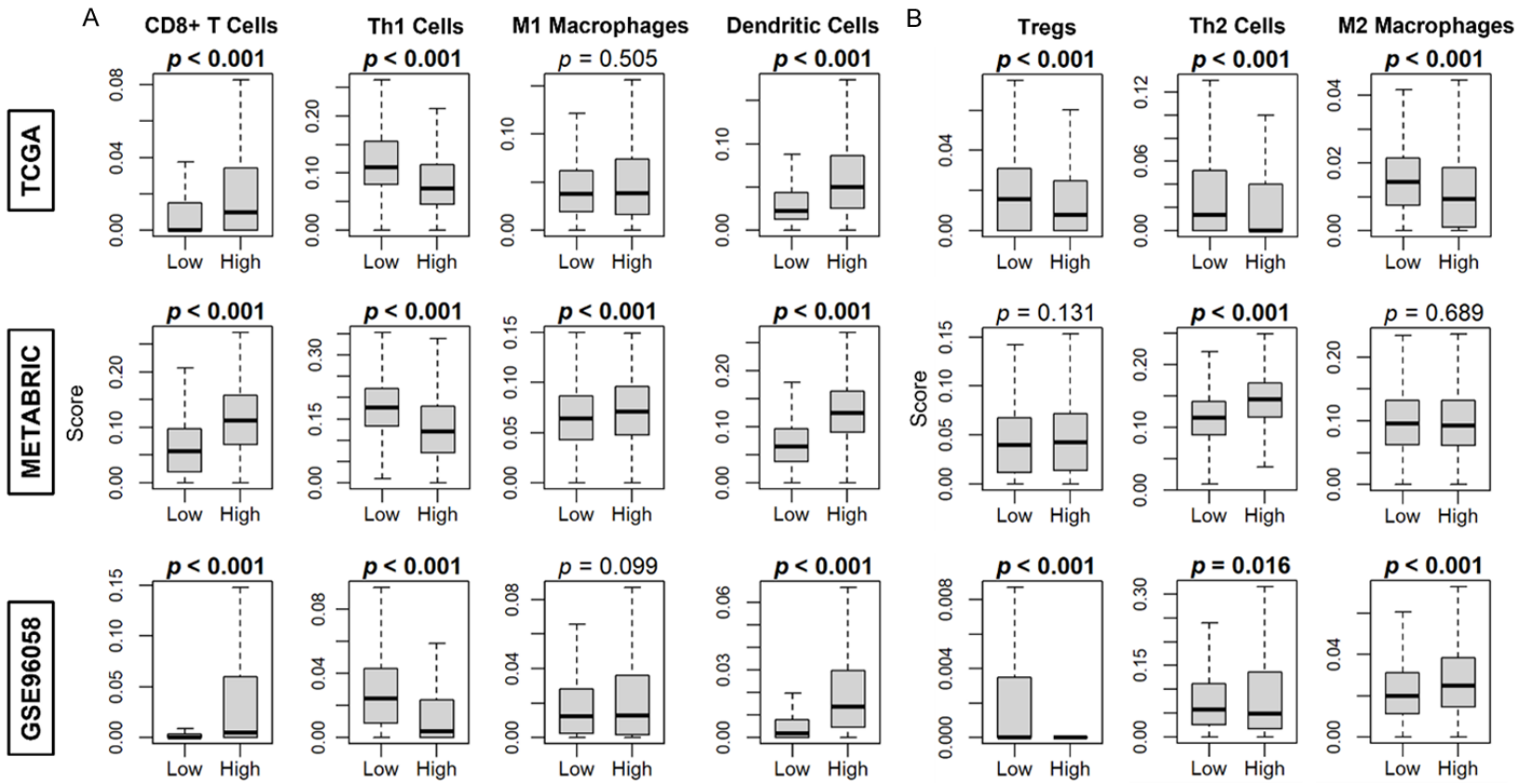

Figure 14. Anti-cancerous and pro-cancerous immune cell correlation with ATX (*ENPP2*) expression in breast cancer tumors. A. Populations of anti-cancerous immune cells. B. Populations of pro-cancerous immune cells. Box plots are based on the xCell algorithm for the TCGA, METABRIC, and GSE96058 cohorts. *ENPP2* expression is dichotomized into low and high groups by the median (total counts by cohort: TCGA - 1090, METABRIC - 1094, GSE96058 - 3609). The bolded center bar represents the median, the lower and upper box bounds represent the 25th and 75th percentiles, respectively, and the lower and upper tails represent the minimum and maximum values, respectively.

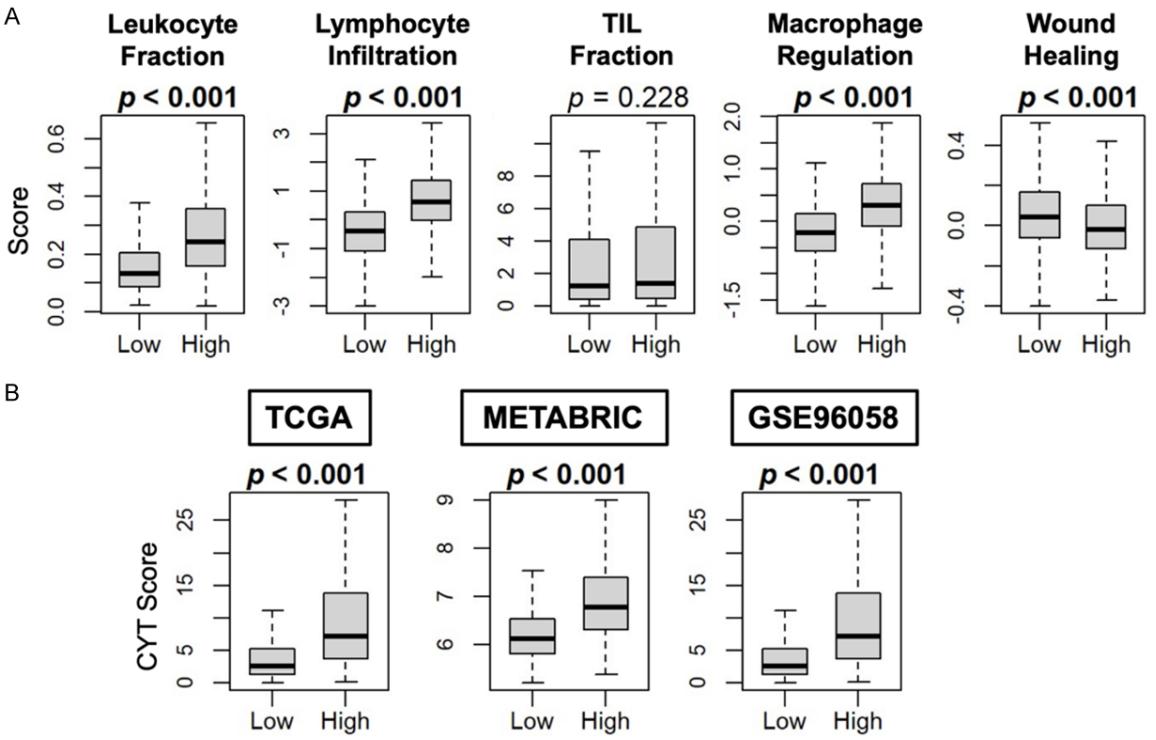

Figure 15. Immune scores for markers of tumor immune cell populations and cytolytic (CYT) score correlation with ATX (*ENPP2*) expression in breast cancer tumors. A. Immune score results are based on score by Thorsson *et al.* [45]. B. CYT scores are calculated using the xCell algorithm. *ENPP2* expression is dichotomized into low and high groups by the median (total counts by cohort: TCGA - 1090, METABRIC - 1094, GSE96058 - 3609). The bolded center bar represents the median, the lower and upper box bounds represent the 25th and 75th percentiles, respectively, and the lower and upper tails represent the minimum and maximum values, respectively.

However, until this publication, there has been no systematic analysis of large cohort level of breast cancer data to verify if models of ATX expression largely derived from pre-clinical studies are robustly relatable to human breast tumors.

In this work, we demonstrate that ATX in human breast tumors is mainly produced by TME cell populations, predominantly endothelial cells, fibroblasts and adipose tissue. We did not observe a difference in ATX expression for different stages and grades, however this is not unexpected because very little ATX is produced by breast cancer cells, and stromal composition correlates poorly with subtype or grade [67]. Virtually all tumors in these three cohorts are early and/or non-metastatic tumors. As such, these tumors can be considered as “early wounds” within the surrounding breast parenchyma [68]. Under such circumstances, ATX produced by the breast stroma is more likely to act in a physiological wound healing capacity to increase infiltration of immune cells into the TME. To support this, we observed decreased Ki67 scores, decreased tumor mutational burden, increased anti-tumor immune cell populations and CYT scores, and trends towards better overall survival with increased tumor ATX expression. High ATX tumor expression in these early tumors was also correlated to increased LPP1/3 and decreased LPP2 expression, which is a phenotype well established to encourage LPA turnover and modulate LPA signaling to within parameters consistent to physiological signaling [10, 69]. Aggressive breast cancers have suppressed LPP1/3 activity leading to decreased turnover of extracellular LPA. This is accompanied by increased LPP2 expression, which promotes the entry of cancer cells into S-phase of the cell cycle through increased c-myc expression [10, 70-72].

Additionally, on GSEA, immune cell, tumor suppressor, and inflammatory related gene sets were upregulated. However, gene sets related to tumor survival and stemness were also enriched, suggesting that breast tumors readily express the signaling ingredients necessary to subvert early pro-healing ATX/LPA signal-

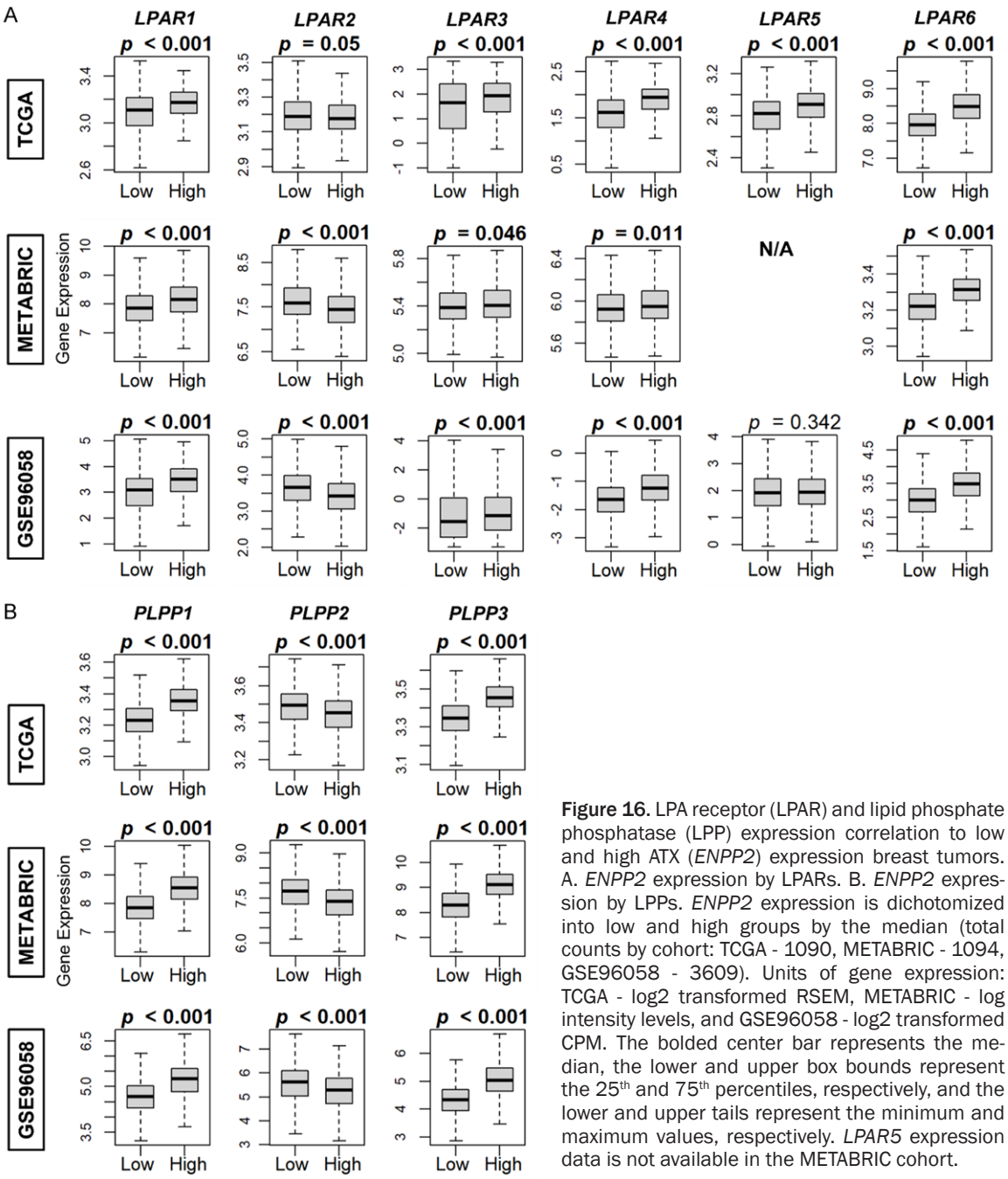

Figure 16. LPA receptor (LPAR) and lipid phosphate phosphatase (LPP) expression correlation to low and high ATX (*ENPP2*) expression breast tumors. A. *ENPP2* expression by LPARs. B. *ENPP2* expression by LPPs. *ENPP2* expression is dichotomized into low and high groups by the median (total counts by cohort: TCGA - 1090, METABRIC - 1094, GSE96058 - 3609). Units of gene expression: TCGA - log2 transformed RSEM, METABRIC - log intensity levels, and GSE96058 - log2 transformed CPM. The bolded center bar represents the median, the lower and upper box bounds represent the 25th and 75th percentiles, respectively, and the lower and upper tails represent the minimum and maximum values, respectively. *LPAR5* expression data is not available in the METABRIC cohort.

ing mechanisms into a pro-carcinogenesis and treatment-survival arsenal. Therefore, the results of this study do not contradict pre-clinical models showing ATX as a promoter of a pro-cancer phenotype, because the vast majority of tumors in the cohorts analyzed in this study are early and treatment naive tumors. By contrast, pre-clinical studies use aggressive, highly metastatic and/or treatment resistant cell lines to demonstrate proof-of-concept ideas. In such tumors, high ATX expression combined with low expression of LPP1 and LPP3 with high LPP2 activities lead to a metastatic phenotype [4, 10].

ATX/LPA signaling inhibitors have tremendous prospects as adjuvants to reduce treatment resistance and treatment side-effects such as radiation-induced fibrosis, and to sensitize tumors to conventional chemotherapy and radiotherapy regimens [4, 11, 73]. However, it is not clear if these inhibitors should be used in early tumors that are treatment naive, in residual tumors following neoadjuvant therapy, and

in cases of disease recurrence. In this study, we were unable to show a correlation between pre-treatment ATX expression and tumor clinical response status to neoadjuvant treatment. Instead, what will be required are serial measurements of ATX mRNA and/or activity, either from tumor tissue, plasma ATX activity, or circulating tumor-free DNA to uncover the temporal nature of ATX signaling in clinical settings.

As a retrospective analysis, our study has several limitations. Despite using three independent cohorts to validate our key findings, patient populations and treatments were heterogeneous with varied outcomes. We cannot necessarily imply mechanisms of action with bioinformatic data, but they can provide insightful support and comparative analysis to existing experimental pre-clinical models. Our study demonstrates that ATX can act as a physiological mediator of wound healing with the immune system attempting to suppress tumorigenesis in early breast tumor growth.

The overarching finding of this study is that ATX is clearly produced by the TME in human breast cancers across all subtypes. This is consistent with the paracrine production model of ATX expression in pre-clinical investigations. However, ATX in patients with early breast cancers appears to mitigate tumor growth: breast tumors with high ATX expression have increased expression of gene sets that also drive tumor stemness and survival against treatment. Therefore, breast cancers appear to have the propensity to hijack ATX signaling for eventual tumorigenesis and treatment resistance as the tumors progress. This finding is already supported by pre-clinical research. Additional research is needed to support this proposed temporal switch in human breast cancer patients. This could support the initiation of clinical trials for oral ATX inhibitors as therapy adjuncts for breast cancer in the setting of advanced tumors or developing treatment resistance.

Acknowledgements

This research was supported by the National Institutes of Health, USA grant numbers R37-CA248018, R01CA250412, R01CA251545, R01EB029596, the US Department of Defense BCRP grant numbers W81XWH-19-1-0674 and W81XWH-19-1-0111 to K.T., and the National Cancer Institute Cancer Center Support Grant P30CA016056 to Roswell Park Comprehensive Cancer Center.

Disclosure of conflict of interest

None.

Address correspondence to: Dr. Kazuaki Takabe, Department of Surgical Oncology, Roswell Park Comprehensive Cancer Center, Elm & Carlton Streets, Buffalo, New York 14263, USA. Tel: +1-716-845-5540; E-mail: kazuaki.takabe@roswellpark.org

References

[1] Siegel RL, Miller KD, Fuchs HE and Jemal A. Cancer statistics, 2022. CA Cancer J Clin 2022; 72: 7-33.

[2] Wang R, Zhu Y, Liu X, Liao X, He J and Niu L. The clinicopathological features and survival outcomes of patients with different metastatic sites in stage IV breast cancer. BMC Cancer 2019; 19: 1091.

[3] Centers for Disease Control and Prevention. U.S. Cancer Statistics Female Breast Cancer Stat Bite. US Department of Health and Human Services; 2022.

[4] Benesch MGK, Tang X and Brindley DN. Autotaxin and breast cancer: towards overcoming treatment barriers and sequelae. Cancers (Basel) 2020; 12: 374.

[5] Lainetti PF, Leis-Filho AF, Laufer-Amorim R, Battazza A and Fonseca-Alves CE. Mechanisms of resistance to chemotherapy in breast cancer and possible targets in drug delivery systems. Pharmaceutics 2020; 12: 1193.

[6] Brindley DN, Tang X, Meng G and Benesch MGK. Role of adipose tissue-derived autotaxin, lysophosphatidate signaling, and inflammation in the progression and treatment of breast cancer. Int J Mol Sci 2020; 21: 5938.

[7] Benesch MGK, Ko YM, McMullen TP and Brindley DN. Autotaxin in the crosshairs: taking aim at cancer and other inflammatory conditions. FEBS Lett 2014; 588: 2712-2727.

[8] Onono FO and Morris AJ. Phospholipase D and choline metabolism. Handb Exp Pharmacol 2020; 259: 205-218.

[9] Lee SC, Fujiwara Y and Tigyi GJ. Uncovering unique roles of LPA receptors in the tumor microenvironment. Receptors Clin Investig 2015; 2: e440.

[10] Tang X, Benesch MG and Brindley DN. Lipid phosphate phosphatases and their roles in mammalian physiology and pathology. J Lipid Res 2015; 56: 2048-2060.

[11] Benesch MGK, MacIntyre ITK, McMullen TPW and Brindley DN. Coming of age for autotaxin and lysophosphatidate signaling: clinical applications for preventing, detecting and targeting

tumor-promoting inflammation. Cancers (Basel) 2018; 10: 73.
[12] Hanahan D and Weinberg RA. Hallmarks of cancer: the next generation. Cell 2011; 144: 646-674.
[13] Colotta F, Allavena P, Sica A, Garlanda C and Mantovani A. Cancer-related inflammation, the seventh hallmark of cancer: links to genetic instability. Carcinogenesis 2009; 30: 1073-1081.
[14] Benesch MGK, Yang Z, Tang X, Meng G and Brindley DN. Lysophosphatidate signaling: the tumor microenvironment's new nemesis. Trends Cancer 2017; 3: 748-752.
[15] So J, Wang FQ, Navari J, Schreher J and Fishman DA. LPA-induced epithelial ovarian cancer (EOC) in vitro invasion and migration are mediated by VEGF receptor-2 (VEGF-R2). Gynecol Oncol 2005; 97: 870-878.
[16] St-Coeur PD, Ferguson D, Morin P Jr and Touaibia M. PF-8380 and closely related analogs: synthesis and structure-activity relationship towards autotaxin inhibition and glioma cell viability. Arch Pharm (Weinheim) 2013; 346: 91-97.
[17] Samadi N, Bekele R, Capatos D, Venkatraman G, Sariahmetoglu M and Brindley DN. Regulation of lysophosphatidate signaling by autotaxin and lipid phosphate phosphatases with respect to tumor progression, angiogenesis, metastasis and chemo-resistance. Biochimie 2011; 93: 61-70.
[18] Euer N, Schwirzke M, Evtimova V, Burtscher H, Jarsch M, Tarin D and Weidle UH. Identification of genes associated with metastasis of mammary carcinoma in metastatic versus non-metastatic cell lines. Anticancer Res 2002; 22: 733-740.
[19] Castellana B, Escuin D, Peiro G, Garcia-Valdecasas B, Vazquez T, Pons C, Perez-Olabarria M, Barnadas A and Lerma E. ASPN and GJB2 are implicated in the mechanisms of invasion of ductal breast carcinomas. J Cancer 2012; 3: 175-183.
[20] Vital AL, Tabernero MD, Castrillo A, Rebelo O, Tao H, Gomes F, Nieto AB, Resende Oliveira C, Lopes MC and Orfao A. Gene expression profiles of human glioblastomas are associated with both tumor cytogenetics and histopathology. Neuro Oncol 2010; 12: 991-1003.
[21] Benesch MG, Tang X, Maeda T, Ohhata A, Zhao YY, Kok BP, Dewald J, Hitt M, Curtis JM, McMullen TP and Brindley DN. Inhibition of autotaxin delays breast tumor growth and lung metastasis in mice. FASEB J 2014; 28: 2655-2666.
[22] Benesch MG, Tang X, Dewald J, Dong WF, Mackey JR, Hemmings DG, McMullen TP and Brindley DN. Tumor-induced inflammation in mammary adipose tissue stimulates a vicious cycle of autotaxin expression and breast cancer progression. FASEB J 2015; 29: 3990-4000.
[23] Jia Y, Li Y, Xu XD, Tian Y and Shang H. Design and development of autotaxin inhibitors. Pharmaceuticals (Basel) 2021; 14: 1203.
[24] Tan Z, Lei H, Guo M, Chen Y and Zhai X. An updated patent review of autotaxin inhibitors (2017-present). Expert Opin Ther Pat 2021; 31: 421-434.
[25] Maher TM, Kreuter M, Lederer DJ, Brown KK, Wuyts W, Verbruggen N, Stutvoet S, Fieuw A, Ford P, Abi-Saab W and Wijsenbeek M. Rationale, design and objectives of two phase III, randomised, placebo-controlled studies of GLPG1690, a novel autotaxin inhibitor, in idiopathic pulmonary fibrosis (ISABELA 1 and 2). BMJ Open Respir Res 2019; 6: e000422.
[26] Helmer E, Willson A, Brearley C, Westerhof M, Delage S, Shaw I, Cooke R and Sidhu S. Pharmacokinetics and metabolism of ziritaxestat (GLPG1690) in healthy male volunteers following intravenous and oral administration. Clin Pharmacol Drug Dev 2022; 11: 246-256.
[27] Iwaki Y, Ohhata A, Nakatani S, Hisaichi K, Okabe Y, Hiramatsu A, Watanabe T, Yamamoto S, Nishiyama T, Kobayashi J, Hirooka Y, Moriguchi H, Maeda T, Katoh M, Komichi Y, Ota H, Matsumura N, Okada M, Sugiyama T, Saga H and Imagawa A. ONO-8430506: a novel autotaxin inhibitor that enhances the antitumor effect of paclitaxel in a breast cancer model. ACS Med Chem Lett 2020; 11: 1335-1341.
[28] Venkatraman G, Benesch MG, Tang X, Dewald J, McMullen TP and Brindley DN. Lysophosphatidate signaling stabilizes Nrf2 and increases the expression of genes involved in drug resistance and oxidative stress responses: implications for cancer treatment. FASEB J 2015; 29: 772-785.
[29] Bekele RT, Venkatraman G, Liu RZ, Tang X, Mi S, Benesch MG, Mackey JR, Godbout R, Curtis JM, McMullen TP and Brindley DN. Oxidative stress contributes to the tamoxifen-induced killing of breast cancer cells: implications for tamoxifen therapy and resistance. Sci Rep 2016; 6: 21164.
[30] Meng G, Wuest M, Tang X, Dufour J, McMullen TPW, Wuest F, Murray D and Brindley DN. Dexamethasone attenuates X-ray-induced activation of the autotaxin-lysophosphatidate-inflammatory cycle in breast tissue and subsequent breast fibrosis. Cancers (Basel) 2020; 12: 999.
[31] Popnikolov NK, Dalwadi BH, Thomas JD, Johannes GJ and Imagawa WT. Association of autotaxin and lysophosphatidic acid receptor 3 with aggressiveness of human breast carcinoma. Tumour Biol 2012; 33: 2237-2243.
[32] Wu R, Yu I, Tokumaru Y, Asaoka M, Oshi M, Yan L, Okuda S, Ishikawa T and Takabe K. Elevated

bile acid metabolism and microbiome are associated with suppressed cell proliferation and better survival in breast cancer. Am J Cancer Res 2022; 12: 5271-5285.
[33] Oshi M, Tokumaru Y, Benesch MG, Sugito N, Wu R, Yan L, Yamada A, Chishima T, Ishikawa T, Endo I and Takabe K. High miR-99b expression is associated with cell proliferation and worse patient outcomes in breast cancer. Am J Cancer Res 2022; 12: 4840-4852.
[34] GTEx Consortium. The genotype-tissue expression (GTEx) project. Nat Genet 2013; 45: 580-585.
[35] Wu SZ, Roden DL, Wang C, Holliday H, Harvey K, Cazet AS, Murphy KJ, Pereira B, Al-Eryani G, Bartonicek N, Hou R, Torpy JR, Junankar S, Chan CL, Lam CE, Hui MN, Gluch L, Beith J, Parker A, Robbins E, Segara D, Mak C, Cooper C, Warrier S, Forrest A, Powell J, O'Toole S, Cox TR, Timpson P, Lim E, Liu XS and Swarbrick A. Stromal cell diversity associated with immune evasion in human triple-negative breast cancer. EMBO J 2020; 39: e104063.
[36] Wu SZ, Al-Eryani G, Roden DL, Junankar S, Harvey K, Andersson A, Thennavan A, Wang C, Torpy JR, Bartonicek N, Wang T, Larsson L, Kaczorowski D, Weisenfeld NI, Uytingco CR, Chew JG, Bent ZW, Chan CL, Gnanasambandapillai V, Dutertre CA, Gluch L, Hui MN, Beith J, Parker A, Robbins E, Segara D, Cooper C, Mak C, Chan B, Warrier S, Ginhoux F, Millar E, Powell JE, Williams SR, Liu XS, O'Toole S, Lim E, Lundeberg J, Perou CM and Swarbrick A. A single-cell and spatially resolved atlas of human breast cancers. Nat Genet 2021; 53: 1334-1347.
[37] Benesch MGK and Mathieson A. Epidemiology of mucinous adenocarcinomas. Cancers (Basel) 2020; 12: 3193.
[38] Subramanian A, Tamayo P, Mootha VK, Mukherjee S, Ebert BL, Gillette MA, Paulovich A, Pomeroy SL, Golub TR, Lander ES and Mesirov JP. Gene set enrichment analysis: a knowledge-based approach for interpreting genome-wide expression profiles. Proc Natl Acad Sci U S A 2005; 102: 15545-15550.
[39] Liberzon A, Birger C, Thorvaldsdóttir H, Ghandi M, Mesirov JP and Tamayo P. The molecular signatures database (MSigDB) hallmark gene set collection. Cell Syst 2015; 1: 417-425.
[40] Aran D, Hu Z and Butte AJ. xCell: digitally portraying the tissue cellular heterogeneity landscape. Genome Biol 2017; 18: 220.
[41] Tokumaru Y, Oshi M, Murthy V, Tian W, Yan L, Angarita FA, Nagahashi M, Matsuhashi N, Futamura M, Yoshida K, Miyoshi Y and Takabe K. Low intratumoral genetic neutrophil-to-lymphocyte ratio (NLR) is associated with favorable tumor immune microenvironment and with survival in triple negative breast cancer (TNBC). Am J Cancer Res 2021; 11: 5743-5755.
[42] Chouliaras K, Oshi M, Asaoka M, Tokumaru Y, Khoury T, Endo I, Ishikawa T and Takabe K. Increased intratumor heterogeneity, angiogenesis and epithelial to mesenchymal transition pathways in metaplastic breast cancer. Am J Cancer Res 2021; 11: 4408-4420.
[43] Le L, Tokumaru Y, Oshi M, Asaoka M, Yan L, Endo I, Ishikawa T, Futamura M, Yoshida K and Takabe K. Th2 cell infiltrations predict neoadjuvant chemotherapy response of estrogen receptor-positive breast cancer. Gland Surg 2021; 10: 154-165.
[44] Oshi M, Asaoka M, Tokumaru Y, Angarita FA, Yan L, Matsuyama R, Zsiros E, Ishikawa T, Endo I and Takabe K. Abundance of regulatory T cell (Treg) as a predictive biomarker for neoadjuvant chemotherapy in triple-negative breast cancer. Cancers (Basel) 2020; 12: 3038.
[45] Thorsson V, Gibbs DL, Brown SD, Wolf D, Bortone DS, Ou Yang TH, Porta-Pardo E, Gao GF, Plaisier CL, Eddy JA, Ziv E, Culhane AC, Paull EO, Sivakumar IKA, Gentles AJ, Malhotra R, Farshidfar F, Colaprico A, Parker JS, Mose LE, Vo NS, Liu J, Liu Y, Rader J, Dhankani V, Reynolds SM, Bowlby R, Califano A, Cherniack AD, Anastassiou D, Bedognetti D, Mokrab Y, Newman AM, Rao A, Chen K, Krasnitz A, Hu H, Malta TM, Noushmehr H, Pedamallu CS, Bullman S, Ojesina AI, Lamb A, Zhou W, Shen H, Choueiri TK, Weinstein JN, Guinney J, Saltz J, Holt RA and Rabkin CS; Cancer Genome Atlas Research Network; Lazar AJ, Serody JS, Demicco EG, Disis ML, Vincent BG and Shmulevich I. The immune landscape of cancer. Immunity 2018; 48: 812-830, e14.
[46] Wakiyama H, Masuda T, Motomura Y, Hu Q, Tobo T, Eguchi H, Sakamoto K, Hirakawa M, Honda H and Mimori K. Cytolytic activity (CYT) score is a prognostic biomarker reflecting host immune status in hepatocellular carcinoma (HCC). Anticancer Res 2018; 38: 6631-6638.
[47] Fusco MJ, West HJ and Walko CM. Tumor mutation burden and cancer treatment. JAMA Oncol 2021; 7: 316.
[48] Stracke ML, Krutzsch HC, Unsworth EJ, Arestad A, Cioce V, Schiffmann E and Liotta LA. Identification, purification, and partial sequence analysis of autotaxin, a novel motility-stimulating protein. J Biol Chem 1992; 267: 2524-2529.
[49] Umezu-Goto M, Kishi Y, Taira A, Hama K, Dohmae N, Takio K, Yamori T, Mills GB, Inoue K, Aoki J and Arai H. Autotaxin has lysophospholipase D activity leading to tumor cell growth and motility by lysophosphatidic acid production. J Cell Biol 2002; 158: 227-233.
[50] Tokumura A, Majima E, Kariya Y, Tominaga K, Kogure K, Yasuda K and Fukuzawa K. Identifi-

cation of human plasma lysophospholipase D, a lysophosphatidic acid-producing enzyme, as autotaxin, a multifunctional phosphodiesterase. J Biol Chem 2002; 277: 39436-39442.
[51] Yang SY, Lee J, Park CG, Kim S, Hong S, Chung HC, Min SK, Han JW, Lee HW and Lee HY. Expression of autotaxin (NPP-2) is closely linked to invasiveness of breast cancer cells. Clin Exp Metastasis 2002; 19: 603-608.
[52] Seifert A, Rau S, Kullertz G, Fischer B and Santos AN. TCDD induces cell migration via NFATc1/ATX-signaling in MCF-7 cells. Toxicol Lett 2009; 184: 26-32.
[53] Samadi N, Gaetano C, Goping IS and Brindley DN. Autotaxin protects MCF-7 breast cancer and MDA-MB-435 melanoma cells against Taxol-induced apoptosis. Oncogene 2009; 28: 1028-1039.
[54] Gaetano CG, Samadi N, Tomsig JL, Macdonald TL, Lynch KR and Brindley DN. Inhibition of autotaxin production or activity blocks lysophosphatidylcholine-induced migration of human breast cancer and melanoma cells. Mol Carcinog 2009; 48: 801-809.
[55] Liu S, Umezu-Goto M, Murph M, Lu Y, Liu W, Zhang F, Yu S, Stephens LC, Cui X, Murrow G, Coombes K, Muller W, Hung MC, Perou CM, Lee AV, Fang X and Mills GB. Expression of autotaxin and lysophosphatidic acid receptors increases mammary tumorigenesis, invasion, and metastases. Cancer Cell 2009; 15: 539-550.
[56] Koike S, Yutoh Y, Keino-Masu K, Noji S, Masu M and Ohuchi H. Autotaxin is required for the cranial neural tube closure and establishment of the midbrain-hindbrain boundary during mouse development. Dev Dyn 2011; 240: 413-421.
[57] van Meeteren LA, Ruurs P, Stortelers C, Bouwman P, van Rooijen MA, Pradere JP, Pettit TR, Wakelam MJ, Saulnier-Blache JS, Mummery CL, Moolenaar WH and Jonkers J. Autotaxin, a secreted lysophospholipase D, is essential for blood vessel formation during development. Mol Cell Biol 2006; 26: 5015-5022.
[58] Brindley DN. Lipid phosphate phosphatases and related proteins: signaling functions in development, cell division, and cancer. J Cell Biochem 2004; 92: 900-912.
[59] Liu S, Murph M, Panupinthu N and Mills GB. ATX-LPA receptor axis in inflammation and cancer. Cell Cycle 2009; 8: 3695-3701.
[60] Panupinthu N, Lee HY and Mills GB. Lysophosphatidic acid production and action: critical new players in breast cancer initiation and progression. Br J Cancer 2010; 102: 941-946.
[61] Meng G, Tang X, Yang Z, Benesch MGK, Marshall A, Murray D, Hemmings DG, Wuest F, McMullen TPW and Brindley DN. Implications for breast cancer treatment from increased autotaxin production in adipose tissue after radiotherapy. FASEB J 2017; 31: 4064-4077.
[62] Meng G, Tang X, Yang Z, Zhao Y, Curtis JM, McMullen TPW and Brindley DN. Dexamethasone decreases the autotaxin-lysophosphatidate-inflammatory axis in adipose tissue: implications for the metabolic syndrome and breast cancer. FASEB J 2019; 33: 1899-1910.
[63] Benesch MGK, Zhao YY, Curtis JM, McMullen TP and Brindley DN. Regulation of autotaxin expression and secretion by lysophosphatidate and sphingosine 1-phosphate. J Lipid Res 2015; 56: 1134-1144.
[64] Drosouni A, Panagopoulou M, Aidinis V and Chatzaki E. Autotaxin in breast cancer: role, epigenetic regulation and clinical implications. Cancers (Basel) 2022; 14: 5437.
[65] Panagopoulou M, Drosouni A, Fanidis D, Karaglani M, Balgkouranidou I, Xenidis N, Aidinis V and Chatzaki E. ENPP2 promoter methylation correlates with decreased gene expression in breast cancer: implementation as a liquid biopsy biomarker. Int J Mol Sci 2022; 23: 3717.
[66] Shao Y, Yu Y, He Y, Chen Q and Liu H. Serum ATX as a novel biomarker for breast cancer. Medicine (Baltimore) 2019; 98: e14973.
[67] Olsson LT, Williams LA, Midkiff BR, Kirk EL, Troester MA and Calhoun BC. Quantitative analysis of breast cancer tissue composition and associations with tumor subtype. Hum Pathol 2022; 123: 84-92.
[68] Dvorak HF. Tumors: wounds that do not heal. Similarities between tumor stroma generation and wound healing. N Engl J Med 1986; 315: 1650-1659.
[69] Tang X, McMullen TPW and Brindley DN. Increasing the low lipid phosphate phosphatase 1 activity in breast cancer cells decreases transcription by AP-1 and expressions of matrix metalloproteinases and cyclin D1/D3. Theranostics 2019; 9: 6129-6142.
[70] Morris KE, Schang LM and Brindley DN. Lipid phosphate phosphatase-2 activity regulates S-phase entry of the cell cycle in Rat2 fibroblasts. J Biol Chem 2006; 281: 9297-9306.
[71] Tang X, Cromwell CR, Liu R, Godbout R, Hubbard BP, McMullen TPW and Brindley DN. Lipid phosphate phosphatase-2 promotes tumor growth through increased c-Myc expression. Theranostics 2022; 12: 5675-5690.
[72] Flanagan JM, Funes JM, Henderson S, Wild L, Carey N and Boshoff C. Genomics screen in transformed stem cells reveals RNASEH2A, PPAP2C, and ADARB1 as putative anticancer drug targets. Mol Cancer Ther 2009; 8: 249-260.
[73] Tang X, Benesch MGK and Brindley DN. Role of the autotaxin-lysophosphatidate axis in the development of resistance to cancer therapy. Biochim Biophys Acta Mol Cell Biol Lipids 2020; 1865: 158716.